HIGH-ORDER NUMERICAL SCHEMES FOR HIGH-SPEED FLOWS

by

MARIA LUISA BAMBOZZI OLIVEIRA

Presented to the Faculty of the Graduate School of

The University of Texas at Arlington in Partial Fulfillment

of the Requirements

for the Degree of

DOCTOR OF PHILOSOPHY

THE UNIVERSITY OF TEXAS AT ARLINGTON

August 2009

ACKNOWLEDGEMENTS

Initially, I would like to thank my research advisor and committee chairman, Dr. Chaoqun Liu, for the incredible support and patience throughout the years.

Also, I would like to thank the other committee members, Dr. Hristo Kojouharov, Dr. Frank Lu, Dr. Hua Shan, and Dr. Jianzhong Su, for their understanding and support.

To the administrative staff of the Department of Mathematics, thank you for the friendly chats and all the encouragements. Cecelia, Kim, Shelley, Vishti, Barbara, Beth and all the work-study students, thank you for all the help. Without you, the Department does not function.

I would like to thank the Department of Mathematics, for the financial support during the long semesters through Graduate Teaching and Research Assistantships, and I would also like to thank the Air Force Research Laboratories at Wright-Patterson Air Force Base, OH, for the summer financial support through the Summer Research Programs in the course of this research.

I cannot thank enough my friends in the Department and those who have already left, for helping me have a life outside of work and study.

To my family: even though you are far in physical distance, I always keep you close in my mind and my heart. Your overwhelming encouragement makes me keep going. Thank you.

Finally, I would like to thank my parents, for everything. Thank you for the advices and thank you for the Sunday evening calls – they mean more than you can imagine.

May 7, 2009

ABSTRACT

HIGH-ORDER NUMERICAL SCHEMES FOR HIGH SPEED FLOWS

Maria Luisa Bambozzi Oliveira, PhD

The University of Texas at Arlington, 2009

Supervising Professor: Chaoqun Liu

A numerical scheme with high order of accuracy is necessary to resolve small length scales in flow transition and turbulence processes. However, numerical simulation for shock-boundary layer interaction, shock-acoustic interaction, porous media flow and multiple phase flow, among others, also require a numerical scheme that can successfully capture discontinuities. To accomplish this, it is essential that an effective shock/discontinuity detector is implemented to reduce damping of physically important high-frequency waves.

In this work, two high-order shock capturing schemes – the Weighted Essentially Non-Oscillatory (WENO) scheme and the Weighted Compact Scheme (WCS) – are investigated. Based on this analysis, a shock/discontinuity detector is developed. Results show that the detector is robust and is capable of detecting strong, weak and oblique shocks or discontinuities.

TABLE OF CONTENTS

LIST OF ILLUSTRATIONS

CHAPTER 1

INTRODUCTION

The numerical simulation of flow transition, turbulence, acoustic and many others have greatly improved in the past decades, partly due to the increasing computational resources that are available, such as high performance computers with a large number of compute nodes, and partly due to improvements in computational methods.

One of the critical problems is the numerical approximation of derivatives for a given data set. The complex, small, length-scale structures require numerical schemes with high resolution and high order of accuracy. High-order compact finite difference schemes [8] have been widely applied for these cases, due to their properties. However, problems that involve both shocks/discontinuities and small length-scale features, such as shock-acoustic interaction, the detonation wave, and shock-turbulence interaction require a numerical scheme that is capable of dealing with both situations for determining the derivatives. The high-order compact finite difference schemes were not originally designed for this purpose. High-order compact schemes require that a tridiagonal or pentadiagonal system of equations be solved. The inverse of a tridiagonal or pentadiagonal matrix is dense, causing the global dependence on the data set. This feature is not suitable for shock capturing.

On the other hand, numerical schemes such as Godunov [3], Roe [17], MUSCL [21], ENO [5], [18], [19] and WENO [6], [9] capture the shock sharply. They are based on upwind or bias upwind technology, which introduces artificial numerical dissipation, and thus are not effective for small length-scale features.

A numerical scheme capable of detecting discontinuities in the function, in its first-, second-, or third-order derivatives, is essential for the problems where both shock and high-

frequency waves are considered important. Many high-order numerical schemes and filters have been combined recently to address this issue [7], [12], [22], but the application of filters to remove non physical oscillations requires the exact location of shocks to avoid the generation of more non physical oscillations. Therefore, the development of a precise shock/discontinuity detector is critical.

The structure of the dissertation is as follows. In Chapter 2, the Navier-Stokes equations, that govern the flow of Newtonian fluids, are derived and transformed to curvilinear coordinates. In Chapter 3, the Weighted Compact Scheme (WCS) and the WENO scheme are described in detail, since they both use the WENO weights as a shock/discontinuity detector. In Chapter 4, a deeper analysis of the properties of the WCS and the WENO scheme is accomplished, including deriving the truncation error and the dissipation and dispersion terms of each scheme. In Chapter 5, the schemes are numerically compared and a new Modified Weighted Compact Scheme (MWCS) is described and analyzed. Finally, in Chapter 6, a new shock/discontinuity detector, the Two-Step detector, is developed and numerical examples are shown.

CHAPTER 2

THE NAVIER-STOKES EQUATIONS

In this Chapter, the Navier-Stokes equations will be derived in non-dimensional form, and then they will be transformed to curvilinear coordinates [1], [2].

2.1 Derivation of the Navier-Stokes Equations

The motion of a fluid is described by the conservation of mass, momentum, and of energy for an arbitrary control volume.

2.1.1 Conservation of Mass (Continuity)

Consider a closed surface S whose position is fixed with relation to the coordinate axes and encloses a volume V completely filled with fluid. Given the density of the fluid ρ at a position $\boldsymbol{x}$ and at time t, the mass of the fluid enclosed by the surface at any instant is given by

$$\int \rho \, dV \, ,$$

and the net rate of which the mass flows outwards across the surface is

$$\int \rho \boldsymbol{u} \cdot \boldsymbol{n} \, dS$$

where $\boldsymbol{n}$ is the unit outward normal of the surface S, and dV and dS are respectively elements of the enclosed volume and of the area of the surrounding surface.

The conservation of mass of the fluid requires that

$$\frac{\partial}{\partial t} \int \rho \, dV = -\int \rho \boldsymbol{u} \cdot \boldsymbol{n} \, dS \, .$$

Then, since the volume V is fixed in space, the differentiation under the integral sign, and the transformation of the surface integral (by the divergence theorem) gives

$$\int \frac{\partial \rho}{\partial t} dV + \int \nabla \cdot (\rho \boldsymbol{u}) dV = 0$$

or

$$\int \left[\frac{\partial \rho}{\partial t} + \nabla \cdot (\rho \boldsymbol{u}) \right] dV = 0 .$$

This relation is valid for all choices of volume V that lies entirely in the fluid, and therefore, if the integrand is continuous in $\boldsymbol{x}$, it must be identically zero everywhere in the fluid. Hence, we obtain

$$\frac{\partial \rho}{\partial t} + \nabla \cdot (\rho \boldsymbol{u}) = 0 . \tag{2.1}$$

2.1.2 Conservation of Momentum (Equation of Motion)

For the conservation of momentum in a control volume, the changes of momentum in this volume must be equal to what is gained or lost through the surface that encloses this volume and what is created or consumed by sources and sinks inside the control volume.

Consider a volume of fluid V enclosed by a surface S, fixed with relation to the coordinate axes. For this body of fluid, the momentum is given by

$$\int \rho \boldsymbol{u} \, dV ,$$

and its rate of change

$$\frac{\partial}{\partial t} \int \rho \boldsymbol{u} \, dV = \int \frac{\partial (\rho \boldsymbol{u})}{\partial t} dV .$$

Now, similar to the conservation of mass, the net rate of what is gained or lost through the surface S is given by

$$\int \rho \boldsymbol{u} (\boldsymbol{u} \cdot \boldsymbol{n}) dS = \int \nabla \cdot (\rho \boldsymbol{u} \otimes \boldsymbol{u}) dV ,$$

using the divergence theorem, where $\otimes$ represents the outer product, that is,

$$\rho \boldsymbol{u} \otimes \boldsymbol{u} = \rho \boldsymbol{u}\boldsymbol{u}^T$$

is a tensor.

If we represent the sources and sinks of forces inside the control volume as ***b***, then the conservation of momentum inside the volume *V* is given by

$$\int \frac{\partial(\rho \boldsymbol{u})}{\partial t} dV = -\int \nabla \cdot (\rho \boldsymbol{u} \otimes \boldsymbol{u}) dV + \int \rho \boldsymbol{b}\, dV \,,$$

or

$$\int \left[\frac{\partial(\rho \boldsymbol{u})}{\partial t} + \nabla \cdot (\rho \boldsymbol{u} \otimes \boldsymbol{u}) - \rho \boldsymbol{b} \right] dV = 0 \,.$$

Since the volume *V* is arbitrary inside the fluid, we must have

$$\frac{\partial(\rho \boldsymbol{u})}{\partial t} + \nabla \cdot (\rho \boldsymbol{u} \otimes \boldsymbol{u}) - \rho \boldsymbol{b} = 0 \,,$$

or

$$\frac{\partial(\rho \boldsymbol{u})}{\partial t} + \nabla \cdot (\rho \boldsymbol{u} \otimes \boldsymbol{u}) = \rho \boldsymbol{b} \,. \tag{2.2}$$

Let us examine more carefully what is ***b***.

2.1.2.1 Forces acting on the fluid

The forces ***b*** may be separated into two types: forces due to surface stresses and body forces, such as gravity. Then, we can write that

$$\rho \boldsymbol{b} = \rho \boldsymbol{f} + (\nabla \cdot \sigma) \,,$$

where ***f*** are the body forces and σ is the stress tensor.

The stress is a measure of the intensity of the total internal forces acting within a body across imaginary internal surfaces, as a reaction to external applied forces and body forces. It can be divided into normal and shear components.

If we assume a Newtonian fluid, that is, there is a linear relation between the stress and the rate of strain of the fluid, then by Stokes (1845),

$$\sigma = -(p - \mu_v \nabla \cdot \boldsymbol{u})\boldsymbol{I} + \mu\left[\nabla \boldsymbol{u} + (\nabla \boldsymbol{u})^T - \frac{2}{3}(\nabla \cdot \boldsymbol{u})\boldsymbol{I}\right],$$

where p is the pressure, μ_v is the bulk viscosity related to the viscosity μ by

$$\mu_v = \lambda + \frac{2}{3}\mu,$$

and according to Stokes' hypothesis, λ is taken to make $\mu_v = 0$. Therefore,

$$\sigma = -p\boldsymbol{I} + \lambda(\nabla \cdot \boldsymbol{u})\boldsymbol{I} + \mu\left[\nabla \boldsymbol{u} + (\nabla \boldsymbol{u})^T\right] = -\left[p + \frac{2}{3}\mu(\nabla \cdot \boldsymbol{u})\right]\boldsymbol{I} + \mu\left[\nabla \boldsymbol{u} + (\nabla \boldsymbol{u})^T\right]. \tag{2.3}$$

Hence, the conservation of momentum equations may be written as

$$\frac{\partial(\rho \boldsymbol{u})}{\partial t} + \nabla \cdot (\rho \boldsymbol{u} \otimes \boldsymbol{u}) = \rho \boldsymbol{f} - \nabla p - \frac{2}{3}\nabla[\mu(\nabla \cdot \boldsymbol{u})] + \nabla\left[\mu\left(\nabla \boldsymbol{u} + (\nabla \boldsymbol{u})^T\right)\right]. \tag{2.4}$$

2.1.3 Conservation of Energy

The conservation of energy for a fluid of volume V contained within a surface S can be determined by analyzing the work being done on this mass of fluid by both volume and surface forces, and also by the heat gained through transfer across the boundary and other sources inside the volume, satisfying the first law of Thermodynamics. The conserved quantity is the *total energy* E, defined as the sum of its internal energy and its kinetic energy per unit mass, or

$$E = e + \frac{\boldsymbol{u} \cdot \boldsymbol{u}}{2},$$

where e is the internal energy per unit mass of the fluid.

The rate of change of the total energy inside the volume V contained within a surface S is given by

$$\frac{\partial}{\partial t}\int \rho E \, dV = \int \frac{\partial(\rho E)}{\partial t} dV,$$

while the net rate of what is gained or lost through the surface is given by

$$\int (\rho E)\boldsymbol{u} \cdot \boldsymbol{n} \, dS = \int \nabla \cdot (\rho E)\boldsymbol{u} \, dV.$$

At the same time, heat may be transferred to the fluid in the volume by molecular conduction through the surface *S*, giving

$$\int (k\nabla T)\cdot \boldsymbol{n}\, dS = \int \nabla\cdot(k\nabla T)\, dV\,,$$

where *T* is the absolute temperature and *k* is the thermal conductivity coefficient of the fluid.

We will now analyze the work being done on the fluid by forces; we can separate them into volume and surface sources. The volume sources include the volume forces $\boldsymbol{f}$, and heat sources q_H other than conduction, such as radiation or heat released by chemical reactions. This gives, for the volume *V*,

$$\int (\rho \boldsymbol{f}\cdot\boldsymbol{u} + q_H)\, dV\,.$$

The surface sources are the result of the work done on the fluid by the internal shear stresses σ acting on the surface of the volume considering that there are no external surface heat sources, giving

$$\int (\sigma\cdot\boldsymbol{u})\cdot\boldsymbol{n} dS = \int \nabla\cdot(\sigma\cdot\boldsymbol{u})\, dV\,.$$

Then, grouping all terms, the energy conservation equation, in integral form, becomes

$$\int \frac{\partial(\rho E)}{\partial t}\, dV + \int \nabla\cdot(\rho E)\boldsymbol{u}\, dV = \int \nabla\cdot(k\nabla T)\, dV + \int (\rho \boldsymbol{f}\cdot\boldsymbol{u} + q_H)\, dV + \int \nabla\cdot(\sigma\cdot\boldsymbol{u})\, dV\,, \qquad (2.5)$$

or

$$\frac{\partial(\rho E)}{\partial t} + \nabla\cdot(\rho E)\boldsymbol{u} - \nabla\cdot(k\nabla T) - \nabla\cdot(\sigma\cdot\boldsymbol{u}) = \rho \boldsymbol{f}\cdot\boldsymbol{u} + q_H\,, \qquad (2.6)$$

with

$$\sigma = -\left[p + \frac{2}{3}\mu(\nabla\cdot\boldsymbol{u})\right]\boldsymbol{I} + \mu\left[\nabla\boldsymbol{u} + (\nabla\boldsymbol{u})^T\right]. \qquad (2.7)$$

2.1.4 Summary of Equations

In the previous subsections, we have derived the equations that satisfy the conservation of mass, the conservation of momentum, and the conservation of energy in a

Newtonian fluid. Together, these equations form the system known as the Navier-Stokes equations:

$$\frac{\partial \rho}{\partial t} + \nabla \cdot (\rho \boldsymbol{u}) = 0;$$

$$\frac{\partial (\rho \boldsymbol{u})}{\partial t} + \nabla \cdot (\rho \boldsymbol{u} \otimes \boldsymbol{u}) = \rho \boldsymbol{f} + (\nabla \cdot \sigma);$$

$$\frac{\partial (\rho E)}{\partial t} + \nabla \cdot (\rho E)\boldsymbol{u} - \nabla \cdot (k \nabla T) - \nabla \cdot (\sigma \cdot \boldsymbol{u}) = \rho \boldsymbol{f} \cdot \boldsymbol{u} + q_H,$$

where

$$E = e + \frac{\boldsymbol{u} \cdot \boldsymbol{u}}{2}$$

and

$$\sigma = -\left[p + \frac{2}{3} \mu (\nabla \cdot \boldsymbol{u}) \right] \boldsymbol{I} + \mu \left[\nabla \boldsymbol{u} + (\nabla \boldsymbol{u})^T \right].$$

If we assume that there are no body forces being applied to the volume of fluid and that there are no heat sources in the volume, then the equations can be rewritten as

$$\frac{\partial \rho}{\partial t} + \nabla \cdot (\rho \boldsymbol{u}) = 0;$$

$$\frac{\partial (\rho \boldsymbol{u})}{\partial t} + \nabla \cdot (\rho \boldsymbol{u} \otimes \boldsymbol{u}) = (\nabla \cdot \sigma); \tag{2.8}$$

$$\frac{\partial (\rho E)}{\partial t} + \nabla \cdot (\rho E)\boldsymbol{u} - \nabla \cdot (k \nabla T) - \nabla \cdot (\sigma \cdot \boldsymbol{u}) = 0,$$

with

$$E = e + \frac{\boldsymbol{u} \cdot \boldsymbol{u}}{2} \tag{2.9}$$

and

$$\sigma = -\left[p + \frac{2}{3} \mu (\nabla \cdot \boldsymbol{u}) \right] \boldsymbol{I} + \mu \left[\nabla \boldsymbol{u} + (\nabla \boldsymbol{u})^T \right]. \tag{2.10}$$

In three dimensions, the system above contains five equations (the conservation of momentum equation becomes three separate equations), while in two dimensions, the system has four equations. Two extra equations are needed to solve the system for the unknown variables ρ, $\boldsymbol{u}$, p, E, and T. These equations are the equation of state, for a thermally perfect gas,

$$p = \rho RT \,, \tag{2.11}$$

where R is a gas constant, and the internal energy equation

$$e = c_v T \,. \tag{2.12}$$

2.2 Non-Dimensional Form

Equations (2.8)-(2.12) can be reduced to a non-dimensional form, to allow characteristic parameters such as Mach number, Reynolds number, and Prandtl number to be varied independently. Also, the flow variables are "normalized", such that their values fall between prescribed limits such as 0 and 1 [1]. This can be achieved by dividing each variable by an appropriate dimensional reference parameter. These reference parameters correspond to some relevant quantity in the flow.

Let us define these reference parameters, where ∞ indicates incoming or free stream values:

L is the characteristic length (for example, the chord length of an airfoil);

V_∞ is the speed;

ρ_∞ is the density;

p_∞ is the pressure;

T_∞ is the temperature;

μ_∞ is the dynamic viscosity;

k_∞ is the thermal conductivity.

With these reference parameters, the non-dimensional variables are given by

$$t = \frac{t^*}{L/V_\infty}, \quad \boldsymbol{x} = \frac{\boldsymbol{x}^*}{L}, \qquad \boldsymbol{u} = \frac{\boldsymbol{u}^*}{V_\infty}, \qquad p = \frac{p^*}{\rho_\infty V_\infty^2}, \qquad \boldsymbol{\sigma} = \frac{\boldsymbol{\sigma}^*}{\rho_\infty V_\infty^2},$$

where * represents the dimensional variables.

The other non-dimensional variables assume that

$$p_\infty = \rho_\infty R T_\infty,$$

giving

$$\rho = \frac{\rho^*}{\rho_\infty}, \quad T = \frac{T^*}{T_\infty}, \quad \mu = \mu(T) = \frac{\mu^*}{\mu_\infty}, \quad k = k(T) = \frac{k^*}{k_\infty}.$$

The dynamic viscosity $\mu(T)$ for an ideal gas is given by Sutherland's law (1893):

$$\mu^*(T^*) = \mu_\infty \left(\frac{T^*}{T_\infty}\right)^{3/2} \frac{T_\infty + C^*}{T^* + C^*},$$

or in non-dimensional form,

$$\mu(T) = T^{3/2} \frac{1 + C}{T + C} \tag{2.13}$$

with

$$C = \frac{C^*}{T_\infty}$$

and $C^* = 110.33\text{K}$ for air.

The total energy E^* can be non-dimensionalized in a form consistent with a thermally perfect gas, with

$$e^* = c_v T^*$$

and

$$E^* = e^* + \frac{\boldsymbol{u}^* \cdot \boldsymbol{u}^*}{2},$$

where c_v is a constant, defined as the specific heat at constant volume. Then

$$e = \frac{e^*}{c_v T_\infty},$$

and so

$$E = \frac{E^*}{c_v T_\infty}.$$

Having defined the reference variables, we can rewrite the equations of section 2.1 in non-dimensional form, obtaining:

$$\frac{\rho_\infty V_\infty}{L}\frac{\partial \rho}{\partial t} + \frac{\rho_\infty V_\infty}{L}\nabla\cdot(\rho \boldsymbol{u}) = 0\,;$$

$$\frac{\rho_\infty V_\infty^2}{L}\frac{\partial(\rho \boldsymbol{u})}{\partial t} + \frac{\rho_\infty V_\infty^2}{L}\left[\nabla\cdot(\rho \boldsymbol{u}\otimes\boldsymbol{u})\right] = \frac{\rho_\infty V_\infty^2}{L}(\nabla\cdot\sigma);$$

$$\frac{\rho_\infty c_v T_\infty V_\infty}{L}\frac{\partial(\rho E)}{\partial t} + \frac{\rho_\infty c_v T_\infty V_\infty}{L}\nabla\cdot(\rho E)\boldsymbol{u} - \frac{k_\infty T_\infty}{L^2}\nabla\cdot(k\nabla T) - \frac{\rho_\infty V_\infty^3}{L}\nabla\cdot(\sigma\cdot\boldsymbol{u}) = 0\,;$$

$$\rho_\infty V_\infty^2\sigma = -\left[\rho_\infty V_\infty^2 p + \frac{2}{3}\frac{\mu_\infty V_\infty}{L}\mu(T)(\nabla\cdot\boldsymbol{u})\right]\boldsymbol{I} + \frac{\mu_\infty V_\infty}{L}\mu(T)\left[\nabla\boldsymbol{u} + (\nabla\boldsymbol{u})^T\right],$$

or, simplifying,

$$\frac{\partial \rho}{\partial t} + \nabla\cdot(\rho \boldsymbol{u}) = 0\,;$$

$$\frac{\partial(\rho \boldsymbol{u})}{\partial t} + \left[\nabla\cdot(\rho \boldsymbol{u}\otimes\boldsymbol{u})\right] = (\nabla\cdot\sigma); \qquad (2.14)$$

$$\frac{\partial(\rho E)}{\partial t} + \nabla\cdot(\rho E)\boldsymbol{u} - \frac{1}{\rho_\infty c_v V_\infty}\frac{k_\infty}{L}\nabla\cdot(k\nabla T) - \frac{1}{c_v T_\infty}\frac{V_\infty^2}{1}\nabla\cdot(\sigma\cdot\boldsymbol{u}) = 0\,;$$

$$\sigma = -\left[p + \frac{2}{3}\frac{\mu_\infty}{\rho_\infty V_\infty L}\mu(T)(\nabla\cdot\boldsymbol{u})\right]\boldsymbol{I} + \frac{\mu_\infty}{\rho_\infty V_\infty L}\mu(T)\left[\nabla\boldsymbol{u} + (\nabla\boldsymbol{u})^T\right].$$

We may define constants for the terms that did not simplify. The Reynolds number is defined as

$$Re = \frac{\rho_\infty V_\infty L}{\mu_\infty},$$

while the Prandtl number evaluated at the reference conditions is given by

$$Pr = \frac{c_p \mu_\infty}{k_\infty}$$

and the Mach number is defined as

$$M_\infty = \frac{V_\infty}{\sqrt{\gamma R T_\infty}}.$$

With the thermodynamic relations for the specific heats c_p and c_v, given by

$$c_p = \gamma c_v \quad \text{and} \quad c_p - c_v = R,$$

we obtain

$$c_v = \frac{R}{\gamma - 1},$$

and so the Navier-Stokes equations in non-dimensional form can be written as

$$\frac{\partial \rho}{\partial t} + \nabla \cdot (\rho \boldsymbol{u}) = 0;$$

$$\frac{\partial (\rho \boldsymbol{u})}{\partial t} + \left[\nabla \cdot (\rho \boldsymbol{u} \otimes \boldsymbol{u})\right] = (\nabla \cdot \sigma); \tag{2.15}$$

$$\frac{\partial (\rho E)}{\partial t} + \nabla \cdot (\rho E)\boldsymbol{u} - \frac{\gamma}{RePr} \nabla \cdot (k(T) \nabla T) - \gamma(\gamma - 1) M_\infty^2 \nabla \cdot (\sigma \cdot \boldsymbol{u}) = 0;$$

$$\sigma = -\left[p + \frac{2}{3} \frac{1}{Re} \mu(T)(\nabla \cdot \boldsymbol{u})\right] \boldsymbol{I} + \frac{1}{Re} \mu(T)\left[\nabla \boldsymbol{u} + (\nabla \boldsymbol{u})^T\right].$$

We can also define the thermal conductivity $k(T)$ by Sutherland's law:

$$k(T) = T^{3/2} \frac{1 + \hat{C}}{T + \hat{C}}. \tag{2.16}$$

If we assume that $\hat{C} = C$ (from equation (2.13)), then we are assuming a constant Prandtl number.

Finally, we non-dimensionalize the equation of state:

$$p^* = \rho^* R T^*,$$

obtaining

$$\rho_\infty V_\infty^2 p = \rho_\infty \rho R T T_\infty$$

or

$$p = \rho T \frac{1}{\gamma M_\infty^2} \Rightarrow \gamma M_\infty^2 p = \rho T \ . \tag{2.17}$$

2.3 Expansion in Curvilinear Coordinates

We will now expand the non-dimensionalized Navier-Stokes equations to curvilinear coordinates. For this, it is necessary to expand first the Navier-Stokes equations in 3D Cartesian coordinates *x*, *y*, and *z*. In vector form, we may write the equations as

$$\frac{\partial \boldsymbol{q}}{\partial t} + \frac{\partial \boldsymbol{F}}{\partial x} + \frac{\partial \boldsymbol{G}}{\partial y} + \frac{\partial \boldsymbol{H}}{\partial z} = \frac{1}{\mathrm{Re}}\left(\frac{\partial \boldsymbol{F_v}}{\partial x} + \frac{\partial \boldsymbol{G_v}}{\partial y} + \frac{\partial \boldsymbol{H_v}}{\partial z} \right), \tag{2.18}$$

where

$$\boldsymbol{q} = \left[\ \rho \quad \rho u \quad \rho v \quad \rho w \quad \rho E \right]^T;$$

$$\boldsymbol{F} = \left[\rho u \quad \left(\rho u^2 + p\right) \quad \rho uv \quad \rho uw \quad \left(\rho E + p\right)u \right]^T;$$

$$\boldsymbol{G} = \left[\rho v \quad \rho uv \quad \left(\rho v^2 + p\right) \quad \rho vw \quad \left(\rho E + p\right)v \right]^T;$$

$$\boldsymbol{H} = \left[\rho w \quad \rho uw \quad \rho vw \quad \left(\rho w^2 + p\right) \quad \left(\rho E + p\right)w \right]^T;$$

$$\boldsymbol{F_v} = \left[0 \quad \sigma_{xx} \quad \sigma_{xy} \quad \sigma_{xz} \quad \left(u\sigma_{xx} + v\sigma_{xy} + w\sigma_{xz} - \frac{1}{(\gamma - 1)PrM_\infty^2} k(T) \frac{\partial T}{\partial x} \right) \right]^T;$$

$$\boldsymbol{G_v} = \left[0 \quad \sigma_{xy} \quad \sigma_{yy} \quad \sigma_{yz} \quad \left(u\sigma_{xy} + v\sigma_{yy} + w\sigma_{yz} - \frac{1}{(\gamma - 1)PrM_\infty^2} k(T) \frac{\partial T}{\partial y} \right) \right]^T;$$

$$\boldsymbol{H_v} = \left[0 \quad \sigma_{xz} \quad \sigma_{yz} \quad \sigma_{zz} \quad \left(u\sigma_{xz} + v\sigma_{yz} + w\sigma_{zz} - \frac{1}{(\gamma - 1)PrM_\infty^2} k(T) \frac{\partial T}{\partial z} \right) \right]^T;$$

$$\sigma_{xx} = \frac{2}{3}\mu(T)\left(2\frac{\partial u}{\partial x} - \frac{\partial v}{\partial y} - \frac{\partial w}{\partial z} \right);$$

$$\sigma_{yy} = \frac{2}{3}\mu(T)\left(-\frac{\partial u}{\partial x} + 2\frac{\partial v}{\partial y} - \frac{\partial w}{\partial z}\right);$$

$$\sigma_{zz} = \frac{2}{3}\mu(T)\left(-\frac{\partial u}{\partial x} - \frac{\partial v}{\partial y} + 2\frac{\partial w}{\partial z}\right);$$

$$\sigma_{xy} = \mu(T)\left(\frac{\partial u}{\partial y} + \frac{\partial v}{\partial x}\right);$$

$$\sigma_{xz} = \mu(T)\left(\frac{\partial u}{\partial z} + \frac{\partial w}{\partial x}\right);$$

$$\sigma_{yz} = \mu(T)\left(\frac{\partial w}{\partial y} + \frac{\partial v}{\partial z}\right).$$

2.3.1 Curvilinear Coordinate Transformation

Let us assume that the position frame of reference is fixed in time, that is, the generalized coordinates do not change with time. Then, we can define the curvilinear coordinates in relation to the Cartesian coordinates as

$$\begin{aligned} \tau &= t; \\ \xi &= \xi(x, y, z); \\ \eta &= \eta(x, y, z); \\ \zeta &= \zeta(x, y, z), \end{aligned} \tag{2.19}$$

such that

$$\frac{\partial}{\partial t} = \frac{\partial}{\partial \tau};$$

$$\frac{\partial}{\partial x} = \frac{\partial \xi}{\partial x}\frac{\partial}{\partial \xi} + \frac{\partial \eta}{\partial x}\frac{\partial}{\partial \eta} + \frac{\partial \zeta}{\partial x}\frac{\partial}{\partial \zeta} = \xi_x \frac{\partial}{\partial \xi} + \eta_x \frac{\partial}{\partial \eta} + \zeta_x \frac{\partial}{\partial \zeta}; \tag{2.20}$$

$$\frac{\partial}{\partial y} = \frac{\partial \xi}{\partial y}\frac{\partial}{\partial \xi} + \frac{\partial \eta}{\partial y}\frac{\partial}{\partial \eta} + \frac{\partial \zeta}{\partial y}\frac{\partial}{\partial \zeta} = \xi_y \frac{\partial}{\partial \xi} + \eta_y \frac{\partial}{\partial \eta} + \zeta_y \frac{\partial}{\partial \zeta};$$

$$\frac{\partial}{\partial z} = \frac{\partial \xi}{\partial z}\frac{\partial}{\partial \xi} + \frac{\partial \eta}{\partial z}\frac{\partial}{\partial \eta} + \frac{\partial \zeta}{\partial z}\frac{\partial}{\partial \zeta} = \xi_z \frac{\partial}{\partial \xi} + \eta_z \frac{\partial}{\partial \eta} + \zeta_z \frac{\partial}{\partial \zeta}.$$

But

$$d\tau = dt;$$

$$d\xi = \xi_x dx + \xi_y dy + \xi_z dz;$$

$$d\eta = \eta_x dx + \eta_y dy + \eta_z dz;$$

$$d\zeta = \zeta_x dx + \zeta_y dy + \zeta_z dz,$$

or

$$\begin{bmatrix} d\tau \\ d\xi \\ d\eta \\ d\zeta \end{bmatrix} = \begin{bmatrix} 1 & 0 & 0 & 0 \\ 0 & \xi_x & \xi_y & \xi_z \\ 0 & \eta_x & \eta_y & \eta_z \\ 0 & \zeta_x & \zeta_y & \zeta_z \end{bmatrix} \begin{bmatrix} dt \\ dx \\ dy \\ dz \end{bmatrix}, \tag{2.21}$$

and

$$dt = d\tau;$$

$$dx = x_\xi d\xi + x_\eta d\eta + x_\zeta d\zeta;$$

$$dy = y_\xi d\xi + y_\eta d\eta + y_\zeta d\zeta;$$

$$dz = z_\xi d\xi + z_\eta d\eta + z_\zeta d\zeta,$$

or

$$\begin{bmatrix} dt \\ dx \\ dy \\ dz \end{bmatrix} = \begin{bmatrix} 1 & 0 & 0 & 0 \\ 0 & x_\xi & x_\eta & x_\zeta \\ 0 & y_\xi & y_\eta & y_\zeta \\ 0 & z_\xi & z_\eta & z_\zeta \end{bmatrix} \begin{bmatrix} d\tau \\ d\xi \\ d\eta \\ d\zeta \end{bmatrix}. \tag{2.22}$$

Then,

$$\begin{bmatrix} 1 & 0 & 0 & 0 \\ 0 & \xi_x & \xi_y & \xi_z \\ 0 & \eta_x & \eta_y & \eta_z \\ 0 & \zeta_x & \zeta_y & \zeta_z \end{bmatrix} = \begin{bmatrix} 1 & 0 & 0 & 0 \\ 0 & x_\xi & x_\eta & x_\zeta \\ 0 & y_\xi & y_\eta & y_\zeta \\ 0 & z_\xi & z_\eta & z_\zeta \end{bmatrix}^{-1}. \tag{2.23}$$

Let us define

$$\begin{aligned} J &= \begin{vmatrix} 1 & 0 & 0 & 0 \\ 0 & \xi_x & \xi_y & \xi_z \\ 0 & \eta_x & \eta_y & \eta_z \\ 0 & \zeta_x & \zeta_y & \zeta_z \end{vmatrix} = \frac{1}{\begin{vmatrix} 1 & 0 & 0 & 0 \\ 0 & x_\xi & x_\eta & x_\zeta \\ 0 & y_\xi & y_\eta & y_\zeta \\ 0 & z_\xi & z_\eta & z_\zeta \end{vmatrix}} = \\ &= 1/\left[x_\xi\left(y_\eta z_\zeta - y_\zeta z_\eta\right) - x_\eta\left(y_\xi z_\zeta - y_\zeta z_\xi\right) + x_\zeta\left(y_\xi z_\eta - y_\eta z_\xi\right)\right]. \end{aligned} \tag{2.24}$$

Therefore,

$$\begin{bmatrix} \xi_x & \xi_y & \xi_z \\ \eta_x & \eta_y & \eta_z \\ \zeta_x & \zeta_y & \zeta_z \end{bmatrix} = J \begin{bmatrix} \left(y_\eta z_\zeta - y_\zeta z_\eta\right) & \left(x_\zeta z_\eta - x_\eta z_\zeta\right) & \left(x_\eta y_\zeta - x_\zeta y_\eta\right) \\ \left(y_\zeta z_\xi - y_\xi z_\zeta\right) & \left(x_\xi z_\zeta - x_\zeta z_\xi\right) & \left(x_\zeta y_\xi - x_\xi y_\zeta\right) \\ \left(y_\xi z_\eta - y_\eta z_\xi\right) & \left(x_\eta z_\xi - x_\xi z_\eta\right) & \left(x_\xi y_\eta - x_\eta y_\xi\right) \end{bmatrix}. \tag{2.25}$$

2.3.2 Navier-Stokes Equations in Curvilinear Coordinates

In vector form, we can write the governing equations in curvilinear coordinates as

$$\begin{aligned} &\frac{\partial \boldsymbol{q}}{\partial \tau} + \xi_x \frac{\partial \boldsymbol{F}}{\partial \xi} + \eta_x \frac{\partial \boldsymbol{F}}{\partial \eta} + \zeta_x \frac{\partial \boldsymbol{F}}{\partial \zeta} + \xi_y \frac{\partial \boldsymbol{G}}{\partial \xi} + \eta_y \frac{\partial \boldsymbol{G}}{\partial \eta} + \zeta_y \frac{\partial \boldsymbol{G}}{\partial \zeta} \\ &+ \xi_z \frac{\partial \boldsymbol{H}}{\partial \xi} + \eta_z \frac{\partial \boldsymbol{H}}{\partial \eta} + \zeta_z \frac{\partial \boldsymbol{H}}{\partial \zeta} = \\ &= \frac{1}{Re}\left(\xi_x \frac{\partial \boldsymbol{F_v}}{\partial \xi} + \eta_x \frac{\partial \boldsymbol{F_v}}{\partial \eta} + \zeta_x \frac{\partial \boldsymbol{F_v}}{\partial \zeta} + \xi_y \frac{\partial \boldsymbol{G_v}}{\partial \xi} + \eta_y \frac{\partial \boldsymbol{G_v}}{\partial \eta} \right. \\ &\left. + \zeta_y \frac{\partial \boldsymbol{G_v}}{\partial \zeta} + \xi_z \frac{\partial \boldsymbol{H_v}}{\partial \xi} + \eta_z \frac{\partial \boldsymbol{H_v}}{\partial \eta} + \zeta_z \frac{\partial \boldsymbol{H_v}}{\partial \zeta} \right). \end{aligned} \tag{2.26}$$

Dividing by J and using metric identities, (2.26) may be written in the following form:

$$\begin{aligned}
&\frac{\partial}{\partial\tau}\left(\frac{\boldsymbol{q}}{J}\right)+\frac{\partial}{\partial\xi}\left(\frac{\xi_x\boldsymbol{F}+\xi_y\boldsymbol{G}+\xi_z\boldsymbol{H}}{J}\right)+\frac{\partial}{\partial\eta}\left(\frac{\eta_x\boldsymbol{F}+\eta_y\boldsymbol{G}+\eta_z\boldsymbol{H}}{J}\right)+\\
&+\frac{\partial}{\partial\zeta}\left(\frac{\zeta_x\boldsymbol{F}+\zeta_y\boldsymbol{G}+\zeta_z\boldsymbol{H}}{J}\right)-\boldsymbol{F}\left[\left(\frac{\xi_x}{J}\right)_\xi+\left(\frac{\eta_x}{J}\right)_\eta+\left(\frac{\zeta_x}{J}\right)_\zeta\right]+\\
&-\boldsymbol{G}\left[\left(\frac{\xi_y}{J}\right)_\xi+\left(\frac{\eta_y}{J}\right)_\eta+\left(\frac{\zeta_y}{J}\right)_\zeta\right]-\boldsymbol{H}\left[\left(\frac{\xi_z}{J}\right)_\xi+\left(\frac{\eta_z}{J}\right)_\eta+\left(\frac{\zeta_z}{J}\right)_\zeta\right]=\\
&=\frac{1}{Re}\left\{\frac{\partial}{\partial\xi}\left(\frac{\xi_x\boldsymbol{F_v}+\xi_y\boldsymbol{G_v}+\xi_z\boldsymbol{H_v}}{J}\right)+\frac{\partial}{\partial\eta}\left(\frac{\eta_x\boldsymbol{F_v}+\eta_y\boldsymbol{G_v}+\eta_z\boldsymbol{H_v}}{J}\right)\right.\\
&\left.+\frac{\partial}{\partial\zeta}\left(\frac{\zeta_x\boldsymbol{F_v}+\zeta_y\boldsymbol{G_v}+\zeta_z\boldsymbol{H_v}}{J}\right)\right\}+\\
&-\frac{1}{Re}\left\{\boldsymbol{F_v}\left[\left(\frac{\xi_x}{J}\right)_\xi+\left(\frac{\eta_x}{J}\right)_\eta+\left(\frac{\zeta_x}{J}\right)_\zeta\right]+\boldsymbol{G_v}\left[\left(\frac{\xi_y}{J}\right)_\xi+\left(\frac{\eta_y}{J}\right)_\eta+\left(\frac{\zeta_y}{J}\right)_\zeta\right]\right.\\
&\left.+\boldsymbol{H_v}\left[\left(\frac{\xi_y}{J}\right)_\xi+\left(\frac{\eta_y}{J}\right)_\eta+\left(\frac{\zeta_y}{J}\right)_\zeta\right]\right\}.
\end{aligned}\tag{2.27}$$

Let us analyze the terms inside all occurrences of $[.]$. By using the definitions in equation (2.25), and considering that $a_{\alpha\beta}=a_{\beta\alpha}$, for $a=x,y,z$ and $\alpha,\beta=\tau,\xi,\eta,\zeta$, we obtain:

$$\left(\frac{\xi_x}{J}\right)_\xi+\left(\frac{\eta_x}{J}\right)_\eta+\left(\frac{\zeta_x}{J}\right)_\zeta=\left(y_\eta z_\zeta-y_\zeta z_\eta\right)_\xi+\left(y_\zeta z_\xi-y_\xi z_\zeta\right)_\eta+\left(y_\xi z_\eta-y_\eta z_\xi\right)_\zeta=$$

$$=\left(\underline{y_{\eta\xi}z_\zeta}+\underline{\underline{y_\eta z_{\zeta\xi}}}-\underline{\underline{y_{\zeta\xi}z_\eta}}-\underline{\underline{y_\zeta z_{\eta\xi}}}\right)+\left(\underline{\underline{y_{\zeta\eta}z_\xi}}+\underline{\underline{y_\zeta z_{\xi\eta}}}-\underline{y_{\xi\eta}z_\zeta}-\underline{\underline{y_\xi z_{\zeta\eta}}}\right)$$

$$+\left(\underline{\underline{y_{\xi\zeta}z_\eta}}-\underline{\underline{y_{\eta\zeta}z_\xi}}+\underline{\underline{y_\xi z_{\eta\zeta}}}-\underline{y_\eta z_{\xi\zeta}}\right)=0;$$

$$\left(\frac{\xi_y}{J}\right)_\xi + \left(\frac{\eta_y}{J}\right)_\eta + \left(\frac{\zeta_y}{J}\right)_\zeta = \left(x_\zeta z_\eta - x_\eta z_\zeta\right)_\xi + \left(x_\xi z_\zeta - x_\zeta z_\xi\right)_\eta + \left(x_\eta z_\xi - x_\xi z_\eta\right)_\zeta =$$

$$= \left(\underline{x_{\zeta\xi} z_\eta} + \underline{\underline{x_\zeta z_{\eta\xi}}} - \underline{\underline{x_{\eta\xi} z_\zeta}} - \underline{\underline{x_\eta z_{\zeta\xi}}}\right) + \left(\underline{\underline{x_{\xi\eta} z_\zeta}} + \underline{\underline{x_\xi z_{\zeta\eta}}} - \underline{\underline{x_{\zeta\eta} z_\xi}} - \underline{x_\zeta z_{\xi\eta}}\right)$$

$$+ \left(\underline{\underline{x_{\eta\zeta} z_\xi}} + \underline{\underline{x_\eta z_{\xi\zeta}}} - \underline{x_{\xi\zeta} z_\eta} - \underline{\underline{x_\xi z_{\eta\zeta}}}\right) = 0;$$

$$\left(\frac{\xi_z}{J}\right)_\xi + \left(\frac{\eta_z}{J}\right)_\eta + \left(\frac{\zeta_z}{J}\right)_\zeta = \left(x_\eta y_\zeta - x_\zeta y_\eta\right)_\xi + \left(x_\zeta y_\xi - x_\xi y_\zeta\right)_\eta + \left(x_\xi y_\eta - x_\eta y_\xi\right)_\zeta =$$

$$= \left(\underline{x_{\eta\xi} y_\zeta} + \underline{\underline{x_\eta y_{\zeta\xi}}} - \underline{\underline{x_{\zeta\xi} y_\eta}} - \underline{\underline{x_\zeta y_{\eta\xi}}}\right) + \left(\underline{\underline{x_{\zeta\eta} y_\xi}} + \underline{\underline{x_\zeta y_{\xi\eta}}} - \underline{x_{\xi\eta} y_\zeta} - \underline{\underline{x_\xi y_{\zeta\eta}}}\right)$$

$$+ \left(\underline{\underline{x_{\xi\zeta} y_\eta}} + \underline{\underline{x_\xi y_{\eta\zeta}}} - \underline{\underline{x_{\eta\zeta} y_\xi}} - \underline{x_\eta y_{\xi\zeta}}\right) = 0.$$

Then, we may write the governing equations as

$$\frac{\partial \hat{\boldsymbol{q}}}{\partial \tau} + \frac{\partial \hat{\boldsymbol{F}}}{\partial \xi} + \frac{\partial \hat{\boldsymbol{G}}}{\partial \eta} + \frac{\partial \hat{\boldsymbol{H}}}{\partial \zeta} = \frac{1}{Re}\left[\frac{\partial \hat{\boldsymbol{F}}_{\boldsymbol{v}}}{\partial \xi} + \frac{\partial \hat{\boldsymbol{G}}_{\boldsymbol{v}}}{\partial \eta} + \frac{\partial \hat{\boldsymbol{H}}_{\boldsymbol{v}}}{\partial \zeta}\right], \tag{2.28}$$

where

$$\hat{\boldsymbol{q}} = \frac{\boldsymbol{q}}{J};.$$

$$\hat{\boldsymbol{F}} = \frac{\xi_x \boldsymbol{F} + \xi_y \boldsymbol{G} + \xi_z \boldsymbol{H}}{J};$$

$$\hat{\boldsymbol{G}} = \frac{\eta_x \boldsymbol{F} + \eta_y \boldsymbol{G} + \eta_z \boldsymbol{H}}{J};$$

$$\hat{\boldsymbol{H}} = \frac{\zeta_x \boldsymbol{F} + \zeta_y \boldsymbol{G} + \zeta_z \boldsymbol{H}}{J};$$

$$\hat{\boldsymbol{F}}_{\boldsymbol{v}} = \frac{\xi_x \boldsymbol{F}_{\boldsymbol{v}} + \xi_y \boldsymbol{G}_{\boldsymbol{v}} + \xi_z \boldsymbol{H}_{\boldsymbol{v}}}{J};$$

$$\hat{\boldsymbol{G}}_{\boldsymbol{v}} = \frac{\eta_x \boldsymbol{F}_{\boldsymbol{v}} + \eta_y \boldsymbol{G}_{\boldsymbol{v}} + \eta_z \boldsymbol{H}_{\boldsymbol{v}}}{J};$$

$$\hat{\boldsymbol{H}}_{\boldsymbol{v}} = \frac{\zeta_x \boldsymbol{F}_{\boldsymbol{v}} + \zeta_y \boldsymbol{G}_{\boldsymbol{v}} + \zeta_z \boldsymbol{H}_{\boldsymbol{v}}}{J}.$$

Now, we can expand the flux vectors and the viscous terms. The flux vectors become

$$\hat{\boldsymbol{F}} = \frac{1}{J}\begin{bmatrix} \xi_x \rho u + \xi_y \rho v + \xi_z \rho w \\ \xi_x \left(\rho u^2 + p\right) + \xi_y \rho uv + \xi_z \rho uw \\ \xi_x \rho uv + \xi_y \left(\rho v^2 + p\right) + \xi_z \rho vw \\ \xi_x \rho uw + \xi_y \rho vw + \xi_z \left(\rho w^2 + p\right) \\ \xi_x (\rho E + p)u + \xi_y (\rho E + p)v + \xi_z (\rho E + p)w \end{bmatrix};$$

$$\hat{\boldsymbol{G}} = \frac{1}{J}\begin{bmatrix} \eta_x \rho u + \eta_y \rho v + \eta_z \rho w \\ \eta_x \left(\rho u^2 + p\right) + \eta_y \rho uv + \eta_z \rho uw \\ \eta_x \rho uv + \eta_y \left(\rho v^2 + p\right) + \eta_z \rho vw \\ \eta_x \rho uw + \eta_y \rho vw + \eta_z \left(\rho w^2 + p\right) \\ \eta_x (\rho E + p)u + \eta_y (\rho E + p)v + \eta_z (\rho E + p)w \end{bmatrix};$$

$$\hat{\boldsymbol{H}} = \frac{1}{J}\begin{bmatrix} \zeta_x \rho u + \zeta_y \rho v + \zeta_z \rho w \\ \zeta_x \left(\rho u^2 + p\right) + \zeta_y \rho uv + \zeta_z \rho uw \\ \zeta_x \rho uv + \zeta_y \left(\rho v^2 + p\right) + \zeta_z \rho vw \\ \zeta_x \rho uw + \zeta_y \rho vw + \zeta_z \left(\rho w^2 + p\right) \\ \zeta_x (\rho E + p)u + \zeta_y (\rho E + p)v + \zeta_z (\rho E + p)w \end{bmatrix},$$

while for the viscous terms, we must first determine the expansion of the stress tensor terms in curvilinear coordinates:

$$\sigma_{xx} = \mu(T)\left[2\left(\xi_x \frac{\partial u}{\partial \xi} + \eta_x \frac{\partial u}{\partial \eta} + \zeta_x \frac{\partial u}{\partial \zeta}\right) - \frac{2}{3}\left(\xi_x \frac{\partial u}{\partial \xi} + \xi_y \frac{\partial v}{\partial \xi} + \xi_z \frac{\partial w}{\partial \xi} + \eta_x \frac{\partial u}{\partial \eta} + \eta_y \frac{\partial v}{\partial \eta} + \eta_z \frac{\partial w}{\partial \eta} + \zeta_x \frac{\partial u}{\partial \zeta} + \zeta_y \frac{\partial v}{\partial \zeta} + \zeta_z \frac{\partial w}{\partial \zeta}\right)\right];$$

$$\sigma_{yy} = \mu(T)\left[2\left(\xi_y \frac{\partial v}{\partial \xi} + \eta_y \frac{\partial v}{\partial \eta} + \zeta_y \frac{\partial v}{\partial \zeta}\right) - \frac{2}{3}\left(\xi_x \frac{\partial u}{\partial \xi} + \xi_y \frac{\partial v}{\partial \xi} + \xi_z \frac{\partial w}{\partial \xi} + \eta_x \frac{\partial u}{\partial \eta} + \eta_y \frac{\partial v}{\partial \eta} + \eta_z \frac{\partial w}{\partial \eta} + \zeta_x \frac{\partial u}{\partial \zeta} + \zeta_y \frac{\partial v}{\partial \zeta} + \zeta_z \frac{\partial w}{\partial \zeta}\right)\right];$$

$$\sigma_{zz} = \mu(T)\left[2\left(\xi_z \frac{\partial w}{\partial \xi} + \eta_z \frac{\partial w}{\partial \eta} + \zeta_z \frac{\partial w}{\partial \zeta}\right) - \frac{2}{3}\left(\xi_x \frac{\partial u}{\partial \xi} + \xi_y \frac{\partial v}{\partial \xi} + \xi_z \frac{\partial w}{\partial \xi} + \eta_x \frac{\partial u}{\partial \eta} + \eta_y \frac{\partial v}{\partial \eta} + \eta_z \frac{\partial w}{\partial \eta} + \zeta_x \frac{\partial u}{\partial \zeta} + \zeta_y \frac{\partial v}{\partial \zeta} + \zeta_z \frac{\partial w}{\partial \zeta}\right)\right];$$

$$\sigma_{xy} = \mu(T)\left(\xi_x \frac{\partial v}{\partial \xi} + \xi_y \frac{\partial u}{\partial \xi} + \eta_x \frac{\partial v}{\partial \eta} + \eta_y \frac{\partial u}{\partial \eta} + \zeta_x \frac{\partial v}{\partial \zeta} + \zeta_y \frac{\partial u}{\partial \zeta}\right);$$

$$\sigma_{xz} = \mu(T)\left(\xi_x \frac{\partial w}{\partial \xi} + \xi_z \frac{\partial u}{\partial \xi} + \eta_x \frac{\partial w}{\partial \eta} + \eta_z \frac{\partial u}{\partial \eta} + \zeta_x \frac{\partial w}{\partial \zeta} + \zeta_z \frac{\partial u}{\partial \zeta}\right);$$

$$\sigma_{yz} = \mu(T)\left(\xi_y \frac{\partial w}{\partial \xi} + \xi_z \frac{\partial v}{\partial \xi} + \eta_y \frac{\partial w}{\partial \eta} + \eta_z \frac{\partial v}{\partial \eta} + \zeta_y \frac{\partial w}{\partial \zeta} + \zeta_z \frac{\partial v}{\partial \zeta}\right).$$

Now, let us define

$$\phi^{(\xi)} = -\frac{2}{3}\mu(T)\left(\xi_x \frac{\partial u}{\partial \xi} + \xi_y \frac{\partial v}{\partial \xi} + \xi_z \frac{\partial w}{\partial \xi}\right);$$

$$\phi^{(\eta)} = -\frac{2}{3}\mu(T)\left(\eta_x \frac{\partial u}{\partial \eta} + \eta_y \frac{\partial v}{\partial \eta} + \eta_z \frac{\partial w}{\partial \eta}\right);$$

$$\phi^{(\zeta)} = -\frac{2}{3}\mu(T)\left(\zeta_x \frac{\partial u}{\partial \zeta} + \zeta_y \frac{\partial v}{\partial \zeta} + \zeta_z \frac{\partial w}{\partial \zeta}\right).$$

Then, to possibly simplify the implementation of the viscous terms, these can be split as follows:

$$\hat{\boldsymbol{F}}_{\boldsymbol{v}} = \boldsymbol{F}_{\boldsymbol{v}}^{(\xi)} + \boldsymbol{F}_{\boldsymbol{v}}^{(\eta)} + \boldsymbol{F}_{\boldsymbol{v}}^{(\zeta)};$$

$$\hat{\boldsymbol{G}}_{\boldsymbol{v}} = \boldsymbol{G}_{\boldsymbol{v}}^{(\xi)} + \boldsymbol{G}_{\boldsymbol{v}}^{(\eta)} + \boldsymbol{G}_{\boldsymbol{v}}^{(\zeta)};$$

$$\hat{\boldsymbol{H}}_{\boldsymbol{v}} = \boldsymbol{H}_{\boldsymbol{v}}^{(\xi)} + \boldsymbol{H}_{\boldsymbol{v}}^{(\eta)} + \boldsymbol{H}_{\boldsymbol{v}}^{(\zeta)},$$

such that

$$\frac{1}{Re}\left[\frac{\partial \hat{\boldsymbol{F}}_{\boldsymbol{v}}}{\partial \xi} + \frac{\partial \hat{\boldsymbol{G}}_{\boldsymbol{v}}}{\partial \eta} + \frac{\partial \hat{\boldsymbol{H}}_{\boldsymbol{v}}}{\partial \zeta}\right] = \frac{1}{Re}\left[\frac{\partial}{\partial \xi}\left(\boldsymbol{v}_1 + \boldsymbol{w}_1\right) + \frac{\partial}{\partial \eta}\left(\boldsymbol{v}_2 + \boldsymbol{w}_2\right) + \frac{\partial}{\partial \zeta}\left(\boldsymbol{v}_3 + \boldsymbol{w}_3\right)\right]$$

where

$$\boldsymbol{v}_1 = \frac{\xi_x \boldsymbol{F_v}^{(\xi)} + \xi_y \boldsymbol{G_v}^{(\xi)} + \xi_z \boldsymbol{H_v}^{(\xi)}}{J};$$

$$\boldsymbol{v}_2 = \frac{\eta_x \boldsymbol{F_v}^{(\eta)} + \eta_y \boldsymbol{G_v}^{(\eta)} + \eta_z \boldsymbol{H_v}^{(\eta)}}{J};$$

$$\boldsymbol{v}_3 = \frac{\zeta_x \boldsymbol{F_v}^{(\zeta)} + \zeta_y \boldsymbol{G_v}^{(\zeta)} + \zeta_z \boldsymbol{H_v}^{(\zeta)}}{J};$$

$$\boldsymbol{w}_1 = \frac{\xi_x \left(\boldsymbol{F_v}^{(\eta)} + \boldsymbol{F_v}^{(\zeta)}\right) + \xi_y \left(\boldsymbol{G_v}^{(\eta)} + \boldsymbol{G_v}^{(\zeta)}\right) + \xi_z \left(\boldsymbol{H_v}^{(\eta)} + \boldsymbol{H_v}^{(\zeta)}\right)}{J};$$

$$\boldsymbol{w}_2 = \frac{\eta_x \left(\boldsymbol{F_v}^{(\xi)} + \boldsymbol{F_v}^{(\zeta)}\right) + \eta_y \left(\boldsymbol{G_v}^{(\xi)} + \boldsymbol{G_v}^{(\zeta)}\right) + \eta_z \left(\boldsymbol{H_v}^{(\xi)} + \boldsymbol{H_v}^{(\zeta)}\right)}{J};$$

$$\boldsymbol{w}_3 = \frac{\zeta_x \left(\boldsymbol{F_v}^{(\xi)} + \boldsymbol{F_v}^{(\eta)}\right) + \zeta_y \left(\boldsymbol{G_v}^{(\xi)} + \boldsymbol{G_v}^{(\eta)}\right) + \zeta_z \left(\boldsymbol{H_v}^{(\xi)} + \boldsymbol{H_v}^{(\eta)}\right)}{J}$$

and

$$\boldsymbol{F_v}^{(\xi)} = \begin{bmatrix} 0 \\ 2\mu(T)\xi_x \dfrac{\partial u}{\partial \xi} + \phi^{(\xi)} \\ \mu(T)\left(\xi_x \dfrac{\partial v}{\partial \xi} + \xi_y \dfrac{\partial u}{\partial \xi}\right) \\ \mu(T)\left(\xi_z \dfrac{\partial u}{\partial \xi} + \xi_x \dfrac{\partial w}{\partial \xi}\right) \\ u f_2^{(\xi)} + v f_3^{(\xi)} + w f_4^{(\xi)} - \dfrac{k\xi_x}{(\gamma-1)PrM_\infty^2} \dfrac{\partial T}{\partial \xi} \end{bmatrix} = \begin{bmatrix} f_1^{(\xi)} \\ f_2^{(\xi)} \\ f_3^{(\xi)} \\ f_4^{(\xi)} \\ f_5^{(\xi)} \end{bmatrix};$$

$$\boldsymbol{F_v}^{(\eta)} = \begin{bmatrix} 0 \\ 2\mu(T)\eta_x \dfrac{\partial u}{\partial \eta} + \phi^{(\eta)} \\ \mu(T)\left(\eta_x \dfrac{\partial v}{\partial \eta} + \eta_y \dfrac{\partial u}{\partial \eta}\right) \\ \mu(T)\left(\eta_z \dfrac{\partial u}{\partial \eta} + \eta_x \dfrac{\partial w}{\partial \eta}\right) \\ u f_2^{(\eta)} + v f_3^{(\eta)} + w f_4^{(\eta)} - \dfrac{k\eta_x}{(\gamma-1)PrM_\infty^2} \dfrac{\partial T}{\partial \eta} \end{bmatrix};$$

$$\boldsymbol{F_v}^{(\zeta)} = \begin{bmatrix} 0 \\ 2\mu(T)\zeta_x \dfrac{\partial u}{\partial \zeta} + \phi^{(\zeta)} \\ \mu(T)\left(\zeta_x \dfrac{\partial v}{\partial \zeta} + \zeta_y \dfrac{\partial u}{\partial \zeta}\right) \\ \mu(T)\left(\zeta_z \dfrac{\partial u}{\partial \zeta} + \zeta_x \dfrac{\partial w}{\partial \zeta}\right) \\ uf_2^{(\zeta)} + vf_3^{(\zeta)} + wf_4^{(\zeta)} - \dfrac{k\zeta_x}{(\gamma-1)\mathrm{Pr}\, M_\infty^2}\dfrac{\partial T}{\partial \zeta} \end{bmatrix};$$

$$\boldsymbol{G_v}^{(\xi)} = \begin{bmatrix} 0 \\ \mu(T)\left(\xi_x \dfrac{\partial v}{\partial \xi} + \xi_y \dfrac{\partial u}{\partial \xi}\right) \\ 2\mu(T)\xi_y \dfrac{\partial v}{\partial \xi} + \phi^{(\xi)} \\ \mu(T)\left(\xi_z \dfrac{\partial v}{\partial \xi} + \xi_y \dfrac{\partial w}{\partial \xi}\right) \\ ug_2^{(\xi)} + vg_3^{(\xi)} + wg_4^{(\xi)} - \dfrac{k\xi_y}{(\gamma-1)PrM_\infty^2}\dfrac{\partial T}{\partial \xi} \end{bmatrix} = \begin{bmatrix} g_1^{(\xi)} \\ g_2^{(\xi)} \\ g_3^{(\xi)} \\ g_4^{(\xi)} \\ g_5^{(\xi)} \end{bmatrix};$$

$$\boldsymbol{G_v}^{(\eta)} = \begin{bmatrix} 0 \\ \mu(T)\left(\eta_x \dfrac{\partial v}{\partial \eta} + \eta_y \dfrac{\partial u}{\partial \eta}\right) \\ 2\mu(T)\eta_y \dfrac{\partial v}{\partial \eta} + \phi^{(\eta)} \\ \mu(T)\left(\eta_z \dfrac{\partial v}{\partial \eta} + \eta_y \dfrac{\partial w}{\partial \eta}\right) \\ ug_2^{(\eta)} + vg_3^{(\eta)} + wg_4^{(\eta)} - \dfrac{k\eta_y}{(\gamma-1)PrM_\infty^2}\dfrac{\partial T}{\partial \eta} \end{bmatrix};$$

$$\boldsymbol{G_v}^{(\zeta)} = \begin{bmatrix} 0 \\ \mu(T)\left(\zeta_x \dfrac{\partial v}{\partial \zeta} + \zeta_y \dfrac{\partial u}{\partial \zeta}\right) \\ 2\mu(T)\zeta_y \dfrac{\partial v}{\partial \zeta} + \phi^{(\zeta)} \\ \mu(T)\left(\zeta_z \dfrac{\partial v}{\partial \zeta} + \zeta_y \dfrac{\partial w}{\partial \zeta}\right) \\ ug_2^{(\zeta)} + vg_3^{(\zeta)} + wg_4^{(\zeta)} - \dfrac{k\zeta_y}{(\gamma-1)PrM_\infty^2}\dfrac{\partial T}{\partial \zeta} \end{bmatrix};$$

$$\boldsymbol{H_v}^{(\xi)} = \begin{bmatrix} 0 \\ \mu(T)\left(\xi_x \dfrac{\partial w}{\partial \xi} + \xi_z \dfrac{\partial u}{\partial \xi}\right) \\ \mu(T)\left(\xi_z \dfrac{\partial v}{\partial \xi} + \xi_y \dfrac{\partial w}{\partial \xi}\right) \\ 2\mu(T)\xi_z \dfrac{\partial w}{\partial \xi} + \phi^{(\xi)} \\ uh_2^{(\xi)} + vh_3^{(\xi)} + wh_4^{(\xi)} - \dfrac{k\xi_z}{(\gamma-1)PrM_\infty^2}\dfrac{\partial T}{\partial \xi} \end{bmatrix} = \begin{bmatrix} h_1^{(\xi)} \\ h_2^{(\xi)} \\ h_3^{(\xi)} \\ h_4^{(\xi)} \\ h_5^{(\xi)} \end{bmatrix};$$

$$\boldsymbol{H_v}^{(\eta)} = \begin{bmatrix} 0 \\ \mu(T)\left(\eta_x \dfrac{\partial w}{\partial \eta} + \eta_z \dfrac{\partial u}{\partial \eta}\right) \\ \mu(T)\left(\eta_z \dfrac{\partial v}{\partial \eta} + \eta_y \dfrac{\partial w}{\partial \eta}\right) \\ 2\mu(T)\eta_z \dfrac{\partial w}{\partial \eta} + \phi^{(\eta)} \\ uh_2^{(\eta)} + vh_3^{(\eta)} + wh_4^{(\eta)} - \dfrac{k\eta_z}{(\gamma-1)PrM_\infty^2}\dfrac{\partial T}{\partial \eta} \end{bmatrix};$$

$$\boldsymbol{H_v}^{(\zeta)} = \begin{bmatrix} 0 \\ \mu(T)\left(\zeta_x \dfrac{\partial w}{\partial \zeta} + \zeta_z \dfrac{\partial u}{\partial \zeta}\right) \\ \mu(T)\left(\zeta_z \dfrac{\partial v}{\partial \zeta} + \zeta_y \dfrac{\partial w}{\partial \zeta}\right) \\ 2\mu(T)\zeta_z \dfrac{\partial w}{\partial \zeta} + \phi^{(\zeta)} \\ uh_2^{(\zeta)} + vh_3^{(\zeta)} + wh_4^{(\zeta)} - \dfrac{k\zeta_z}{(\gamma-1)PrM_\infty^2}\dfrac{\partial T}{\partial \zeta} \end{bmatrix}.$$

CHAPTER 3

THE WEIGHTED ESSENTIALLY NON-OSCILLATORY SCHEME AND THE WEIGHTED COMPACT SCHEME

The Weighted Essentially Non-Oscillatory (WENO) scheme [6],[9] and the Weighted Compact Scheme (WCS) [7] are high-order schemes that were designed to capture shock accurately and maintain high order in regions away from shocks. In this Chapter, we will describe in detail the derivation of the numerical schemes.

3.1 Scheme Formulations

Consider the scalar conservation equation

$$u_t(x,t) + F_x(u(x,t)) = 0\,. \tag{3.1}$$

A semi-discrete conservative form of (3.1) can be described as follows:

$$\frac{du_j}{dt} = -\frac{1}{h}\left(\hat{F}_{j+(1/2)} - \hat{F}_{j-(1/2)}\right), \tag{3.2}$$

where $F_j \equiv F\left(u\left(x_j,t\right)\right) = \frac{1}{h}\int_{x_j-h/2}^{x_j+h/2}\hat{F}\left(\xi\right)d\xi$ and h is the step size in the x-direction. Here, F is the original function, but $\hat{F}$ is the flux defined by the integration. Then, (3.2) is an exact expression of (3.1), but $\hat{F}$ is not the same as F.

If we take H as the primitive function of $\hat{F}$, then we can define it as:

$$H\left(x_{j+1/2}\right) = \int_{-\infty}^{x_j+h/2}\hat{F}\left(\xi\right)d\xi = \sum_{i=-\infty}^{j}\int_{x_i-h/2}^{x_i+h/2}\hat{F}(\xi)d\xi = h\sum_{i=-\infty}^{j}F_i\ . \tag{3.3}$$

Here, the numerical flux $\hat{F}$ at the cell interfaces is the derivative of the primitive function H, that is, $H'_{j+1/2} = \hat{F}_{j+1/2}$, and H is to be calculated on discrete data sets. With this information, we can

determine the approximations of $\hat{F}_{j+1/2}$ and $\hat{F}_{j-1/2} = \hat{F}_{(j-1)+1/2}$ for the WENO Scheme and for the WCS, and thus determine $\frac{du_j}{dt}$ in (3.2).

3.2 The 5th Order WENO Scheme

The 5th-order WENO scheme consists of the weighted average of three second-order approximations for the numerical flux, such that the weights are determined according to the "smoothness" of each stencil. To obtain the second-order approximation for $\hat{F}_{j+1/2}$, three candidate stencils are used (Figure 3.1):

$$E_0 : F_{j-2}, F_{j-1}, F_j ; \qquad E_1 : F_{j-1}, F_j, F_{j+1}; \qquad E_2 : F_j, F_{j+1}, F_{j+2} .$$

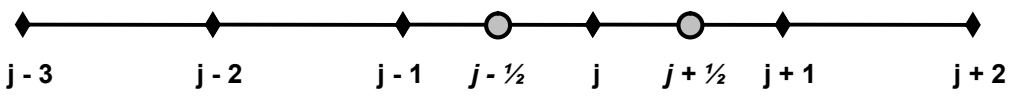

Figure 3.1 5th order WENO scheme diagram

Then, for candidate E_0, the second-order Lagrange polynomial is given by

$$p_{0,j+1/2}(x) = -\frac{F_{j-2} - 26F_{j-1} + F_j}{24} + \frac{F_j - F_{j-2}}{2h}(x - x_{j-1}) + \frac{F_{j-2} - 2F_{j-1} + F_j}{2h^2}(x - x_{j-1})^2 .$$

If we replace $x = x_{j+1/2}$, then the approximation for $\hat{F}_{j+1/2} = p_{0,j+1/2}(x_{j+1/2})$ is:

$$\hat{F}_{j+1/2} = \frac{1}{3}F_{j-2} - \frac{7}{6}F_{j-1} + \frac{11}{6}F_j . \tag{3.4}$$

Similarly, for candidates E_1 and E_2, we obtain:

E_1 :

$$p_{1,j+1/2}(x) = -\frac{F_{j-1} - 26F_j + F_{j+1}}{24} + \frac{F_{j+1} - F_{j-1}}{2h}(x - x_j) + \frac{F_{j-1} - 2F_j + F_{j+1}}{2h^2}(x - x_j)^2$$

$$\hat{F}_{j+1/2} = -\frac{1}{6}F_{j-1} + \frac{5}{6}F_j + \frac{1}{3}F_{j+1}; \tag{3.5}$$

E_2 :

$$p_{2,j+1/2}(x) = -\frac{F_j - 26F_{j+1} + F_{j+2}}{24} + \frac{F_{j+2} - F_j}{2h}\left(x - x_{j+1}\right) + \frac{F_j - 2F_{j+1} + F_{j+2}}{2h^2}\left(x - x_{j+1}\right)^2$$

$$\hat{F}_{j+1/2} = \frac{1}{3}F_j + \frac{5}{6}F_{j+1} - \frac{1}{6}F_{j+2}. \tag{3.6}$$

If a weighted average of the three stencils is considered, with constant weights

$$C_0 = \frac{1}{10}; \quad C_1 = \frac{6}{10}; \quad C_2 = \frac{3}{10}, \tag{3.7}$$

such that

$$E = C_0E_0 + C_1E_1 + C_2E_2, \tag{3.8}$$

then

$$\hat{F}_{j+1/2} = \frac{1}{30}F_{j-2} - \frac{13}{60}F_{j-1} + \frac{47}{60}F_j + \frac{9}{20}F_{j+1} - \frac{1}{20}F_{j+2}. \tag{3.9}$$

Similar derivation for $\hat{F}_{j-1/2} = \hat{F}_{(j-1)+1/2}$ gives

$$\hat{F}_{j-1/2} = \frac{1}{30}F_{j-3} - \frac{13}{60}F_{j-2} + \frac{47}{60}F_{j-1} + \frac{9}{20}F_j - \frac{1}{20}F_{j+1}. \tag{3.10}$$

Therefore, by (3.9) and (3.10),

$$F'_j \approx \frac{\hat{F}_{j+\frac{1}{2}} - \hat{F}_{j-\frac{1}{2}}}{h} = \frac{\left(-\frac{1}{30}F_{j-3} + \frac{1}{4}F_{j-2} - F_{j-1} + \frac{1}{3}F_j + \frac{1}{2}F_{j+1} - \frac{1}{20}F_{j+2}\right)}{h}. \tag{3.11}$$

By using the Taylor expansion, we can verify that (3.11) is $O\left(h^5\right)$:

$$F_j' - \frac{\hat{F}_{j+\frac{1}{2}} - \hat{F}_{j-\frac{1}{2}}}{h} = \frac{1}{60}h^5F_j^{(6)} - \frac{1}{140}h^6F_j^{(7)} + \frac{1}{240}h^7F_j^{(8)} + \ldots \tag{3.12}$$

The use of the constant weights C_0, C_1, and C_2 does not allow for an adaptive scheme according to the "smoothness" of the stencils. A modification to weights $\omega_{0,j\pm1/2}$, $\omega_{1,j\pm1/2}$, and $\omega_{2,j\pm1/2}$ defined in [6] as

$$\omega_{i,j\pm1/2}=\frac{\alpha_{i,j\pm1/2}}{\sum_{k=0}^{2}\alpha_{k,j\pm1/2}};\quad \alpha_{i,j\pm1/2}=\frac{C_i}{\left(\varepsilon+IS_{i,j\pm1/2}\right)^p},\quad i=0,1,2\,, \tag{3.13}$$

where ε is a small quantity to avoid division by zero, p is an integer (equal to 2 in [6]), and $IS_{i,j\pm1/2}$ is a "smoothness" indicator, calculated by $IS_{i,j\pm1/2}=\int_{x_{j-1/2}}^{x_{j+1/2}}\sum_{k=1}^{2}\left(p_{i,j\pm1/2}{}^{(k)}(x)\right)^2 h^{2k-1}dx$:

$$\begin{aligned}
IS_{0,j+1/2}&=\frac{13}{12}\left(F_{j-2}-2F_{j-1}+F_j\right)^2+\frac{1}{4}\left(F_{j-2}-4F_{j-1}+3F_j\right)^2;\\
IS_{1,j+1/2}&=\frac{13}{12}\left(F_{j-1}-2F_j+F_{j+1}\right)^2+\frac{1}{4}\left(F_{j-1}-F_{j+1}\right)^2;\\
IS_{2,j+1/2}&=\frac{13}{12}\left(F_j-2F_{j+1}+F_{j+2}\right)^2+\frac{1}{4}\left(F_{j+2}-4F_{j+1}+3F_j\right)^2,
\end{aligned} \tag{3.14}$$

with similar formulation for $IS_{0,j-1/2}=IS_{0,(j-1)+1/2}$, $IS_{1,j-1/2}=IS_{1,(j-1)+1/2}$, and $IS_{2,j-1/2}=IS_{2,(j-1)+1/2}$, gives an adaptive scheme. Note that $IS_{k,j+1/2}\neq IS_{k,j-1/2}$, in general, and so we consider $\omega_{k,j+1/2}\neq\omega_{k,j-1/2}$, $k=0,1,2$.

With these new weights, we can construct $\hat{F}_{j+1/2}$ and $\hat{F}_{j-1/2}$. With the new weighted average, we have, for the WENO scheme,

$$\begin{aligned}
F'_j\approx\frac{\hat{F}_{j+\frac{1}{2}}-\hat{F}_{j-\frac{1}{2}}}{h}=\Bigg[&-\frac{1}{3}\omega_{0,j-1/2}F_{j-3}+\left(\frac{7}{6}\omega_{0,j-1/2}+\frac{1}{3}\omega_{0,j+1/2}+\frac{1}{6}\omega_{1,j-1/2}\right)F_{j-2}\\
&+\left(-\frac{11}{6}\omega_{0,j-1/2}-\frac{7}{6}\omega_{0,j+1/2}-\frac{5}{6}\omega_{1,j-1/2}-\frac{1}{6}\omega_{1,j+1/2}-\frac{1}{3}\omega_{2,j-1/2}\right)F_{j-1}\\
&+\left(\frac{11}{6}\omega_{0,j+1/2}-\frac{1}{3}\omega_{1,j-1/2}+\frac{5}{6}\omega_{1,j+1/2}-\frac{5}{6}\omega_{2,j-1/2}+\frac{1}{3}\omega_{2,j+1/2}\right)F_j\\
&+\left(\frac{1}{3}\omega_{1,j+1/2}+\frac{1}{6}\omega_{2,j-1/2}+\frac{5}{6}\omega_{2,j+1/2}\right)F_{j+1}-\frac{1}{6}\omega_{2,j+1/2}F_{j+2}\Bigg]\Big/h
\end{aligned}. \tag{3.15}$$

3.3 The Weighted Compact Scheme (WCS)

The WCS idea [7] is to use the weighted average of two third-order and one fourth-order approximation for the numerical flux, where each approximation involves the primitive function H

(see (3.3)) and its derivative at different points, constructed by Hermite polynomials. To obtain the approximations for $\hat{F}_{j+1/2}$, three candidate stencils are used (Figure 3.2):

$$E_0 : H_{j-3/2}, H_{j-1/2}, H_{j+1/2}; \qquad E_1 : H_{j-1/2}, H_{j+1/2}, H_{j+3/2}; \qquad E_2 : H_{j+1/2}, H_{j+3/2}, H_{j+5/2}.$$

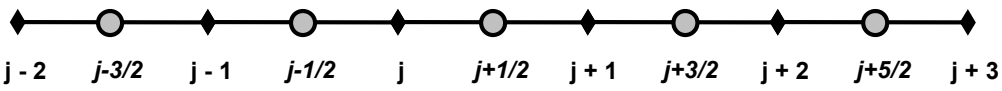

Figure 3.2 Weighted Compact Scheme diagram

Then, according to [8], we can write, for each stencil E_0, E_1, and E_2:

E_0 :

$$2H'_{j-1/2} + H'_{j+1/2} \approx \left(-\frac{1}{2}H_{j-3/2} - 2H_{j-1/2} + \frac{5}{2}H_{j+1/2} \right) \Big/ h; \tag{3.16}$$

E_1 :

$$\frac{1}{4}H'_{j-1/2} + H'_{j+1/2} + \frac{1}{4}H'_{j+3/2} \approx \frac{3\left(H_{j+3/2} - H_{j-1/2}\right)}{4h}; \tag{3.17}$$

E_2 :

$$H'_{j+1/2} + 2H'_{j+3/2} \approx \left(\frac{1}{2}H_{j+5/2} + 2H_{j+3/2} - \frac{5}{2}H_{j+1/2} \right) \Big/ h. \tag{3.18}$$

It can be noted that E_0 and E_2 have third-order accuracy, while E_1 has fourth-order accuracy:

E_0 :

$$2H'_{j-1/2} + H'_{j+1/2} - \left(-\frac{1}{2}H_{j-3/2} - 2H_{j-1/2} + \frac{5}{2}H_{j+1/2} \right) \Big/ h = ;$$
$$= \frac{1}{12}h^3 H^{(4)}_{j+1/2} - \frac{1}{15}h^4 H^{(5)}_{j+1/2} + \frac{11}{360}h^5 H^{(6)}_{j+1/2} + \ldots$$

E_1 :

$$\frac{1}{4}H'_{j-1/2}+H'_{j+1/2}+\frac{1}{4}H'_{j+3/2}-\frac{3\left(H_{j+3/2}-H_{j-1/2}\right)}{4h}=\frac{1}{120}h^4H^{(5)}_{j+1/2}+\frac{1}{2520}h^6H^{(7)}_{j+1/2}+\ldots;$$

E_2 :

$$H'_{j+1/2}+2H'_{j+3/2}-\left(\frac{1}{2}H_{j+5/2}+2H_{j+3/2}-\frac{5}{2}H_{j+1/2}\right)\Big/h=$$
$$=-\frac{1}{12}h^3H^{(4)}_{j+1/2}-\frac{1}{15}h^4H^{(5)}_{j+1/2}-\frac{11}{360}h^5H^{(6)}_{j+1/2}+\ldots$$

As with WENO, if a weighted average of the three stencils is considered, with different constant weights

$$C_0=\frac{1}{18};\quad C_1=\frac{8}{9};\quad C_2=\frac{1}{18},$$

such that

$$E=C_0E_0+C_1E_1+C_2E_2,$$

by (3.16), (3.17) and (3.18), we have for j + 1/2:

$$\left(2C_0+\frac{1}{4}C_1\right)H'_{j-1/2}+\left(C_0+C_1+C_2\right)H'_{j+1/2}+\left(\frac{1}{4}C_1+2C_2\right)H'_{j+3/2}\approx$$
$$\approx\left[-\left(\frac{1}{2}C_0\right)H_{j-3/2}-\left(2C_0+\frac{3}{4}C_1\right)H_{j-1/2}+\frac{5}{2}\left(C_0-C_2\right)H_{j+1/2}+\right.$$
$$\left.+\left(\frac{3}{4}C_1+2C_2\right)H_{j+3/2}+\left(\frac{1}{2}C_2\right)H_{j+5/2}\right]\Big/h$$

or

$$\frac{1}{3}H'_{j-1/2}+H'_{j+1/2}+\frac{1}{3}H'_{j+3/2}\approx$$
$$\approx\left[-\frac{1}{36}H_{j-3/2}-\frac{7}{9}H_{j-1/2}+\frac{7}{9}H_{j+3/2}+\frac{1}{36}H_{j+5/2}\right]\Big/h. \qquad (3.19)$$

Similarly, for *j – 1/2 = (j-1) + 1/2* :

$$\frac{1}{3}H'_{j-3/2}+H'_{j-1/2}+\frac{1}{3}H'_{j+1/2}\approx$$
$$\approx\left[-\frac{1}{36}H_{j-5/2}-\frac{7}{9}H_{j-3/2}+\frac{7}{9}H_{j+1/2}+\frac{1}{36}H_{j+3/2}\right]\Big/h. \qquad (3.20)$$

Since $F_j^{'} = \dfrac{\hat{F}_{j+1/2} - \hat{F}_{j-1/2}}{h} = \dfrac{H_{j+1/2}^{'} - H_{j-1/2}^{'}}{h}$, then $H_{j-1/2}^{'} = H_{j+1/2}^{'} - hF_j^{'}$ and also $H_{j+3/2}^{'} = H_{j+1/2}^{'} + hF_{j+1}^{'}$. Then, subtracting equation (3.20) from equation (3.19), and by (3.3),

$$\begin{aligned} &\frac{1}{3}F_{j-1}^{'} + F_j^{'} + \frac{1}{3}F_{j+1}^{'} \approx \\ &\approx \left(-\frac{1}{36}F_{j-2} - \frac{7}{9}F_{j-1} + \frac{7}{9}F_{j+1} + \frac{1}{36}F_{j+2} \right) \Big/ h \end{aligned} \qquad (3.21)$$

which is a *standard* compact scheme of sixth order. By Taylor series expansion,

$$\begin{aligned} &\frac{1}{3}F_{j-1}^{'} + F^{'}{}_j + \frac{1}{3}F_{j+1}^{'} - \frac{1}{h}\left(-\frac{1}{36}F_{j-2} - \frac{7}{9}F_{j-1} + \frac{7}{9}F_{j+1} + \frac{1}{36}F_{j+2} \right) = \\ &= -\frac{1}{1260}h^6 F_j^{(7)} - \frac{1}{15120}h^8 F_j^{(9)} + \ldots \end{aligned}$$

If WENO weights (3.13) are used instead of the current C_0, C_1, and C_2, with p = 1, then we obtain, for the WCS,

$$\begin{aligned} &-\left(2\omega_{0,j-1/2} + \frac{1}{4}\omega_{1,j-1/2} \right) H_{j-3/2}^{'} + \left(2\omega_{0,j+1/2} + \frac{1}{4}\omega_{1,j+1/2} - 1 \right) H_{j-1/2}^{'} + \\ &+ \left(1 - \frac{1}{4}\omega_{1,j-1/2} - 2\omega_{2,j-1/2} \right) H_{j+1/2}^{'} + \left(\frac{1}{4}\omega_{1,j+1/2} + 2\omega_{2,j+1/2} \right) H_{j+3/2}^{'} \approx \\ &\approx \left[\left(\frac{1}{2}\omega_{0,j-1/2} \right) H_{j-5/2} + \left(2\omega_{0,j-1/2} + \frac{3}{4}\omega_{1,j-1/2} - \frac{1}{2}\omega_{0,j+1/2} \right) H_{j-3/2} + \right. \\ &+ \left(-\frac{5}{2}\omega_{0,j-1/2} + \frac{5}{2}\omega_{2,j-1/2} - 2\omega_{0,j+1/2} - \frac{3}{4}\omega_{1,j+1/2} \right) H_{j-1/2} + \\ &+ \left(-\frac{3}{4}\omega_{1,j-1/2} - 2\omega_{2,j-1/2} + \frac{5}{2}\omega_{0,j+1/2} - \frac{5}{2}\omega_{2,j+1/2} \right) H_{j+1/2} + \\ &\left. + \left(-\frac{1}{2}\omega_{2,j-1/2} + \frac{3}{4}\omega_{1,j+1/2} + 2\omega_{2,j+1/2} \right) H_{j+3/2} + \left(\frac{1}{2}\omega_{2,j+1/2} \right) H_{j+5/2} \right] \Big/ h \end{aligned}$$

or

$$\left(-3\omega_{0,j-1/2}-\frac{3}{2}\omega_{1,j-1/2}-3\omega_{2,j-1/2}+3\omega_{0,j+1/2}+\frac{3}{2}\omega_{1,j+1/2}+3\omega_{2,j+1/2}\right)\frac{H'_{j+1/2}}{h}+$$
$$+\left(2\omega_{0,j-1/2}+\frac{1}{4}\omega_{1,j-1/2}\right)F'_{j-1}+$$
$$+\left(3\omega_{0,j-1/2}+\frac{5}{4}\omega_{1,j-1/2}+\omega_{2,j-1/2}-2\omega_{0,j+1/2}-\frac{1}{4}\omega_{1,j+1/2}\right)F'_{j}+$$
$$+\left(\frac{1}{4}\omega_{1,j+1/2}+2\omega_{2,j+1/2}\right)F'_{j+1}\approx$$
$$\approx\left[-\frac{1}{2}\omega_{0,j-1/2}F_{j-2}+\left(-\frac{5}{2}\omega_{0,j-1/2}-\frac{3}{4}\omega_{1,j-1/2}+\frac{1}{2}\omega_{0,j+1/2}\right)F_{j-1}+\right.$$
$$+\left(-\frac{3}{4}\omega_{1,j-1/2}-\frac{5}{2}\omega_{2,j-1/2}+\frac{5}{2}\omega_{0,j+1/2}+\frac{3}{4}\omega_{1,j+1/2}\right)F_{j}+$$
$$+\left(-\frac{1}{2}\omega_{2,j-1/2}+\frac{3}{4}\omega_{1,j+1/2}+\frac{5}{2}\omega_{2,j+1/2}\right)F_{j+1}+$$
$$\left.+\frac{1}{2}\omega_{2,j+1/2}F_{j+2}\right]\Big/h \qquad (3.22)$$

By the use of derivatives, this shows a global dependency of all values, that is, the solution of the system of equations is dependent on all values of *F*.

CHAPTER 4

ANALYSIS OF LOCAL TRUNCATION ERROR, DISSIPATION AND DISPERSION TERMS OF WENO AND WCS

In this Chapter, a detailed analysis of the local truncation errors, the dissipation and dispersion terms is done for the 5th-order WENO scheme and the Weighted Compact Scheme. A Fourier analysis and an investigation near shocks are performed on both schemes.

4.1 Local Truncation Error, Dissipation and Dispersion Terms

The WENO scheme gives, from equation (3.15),

$$F'_j \approx \frac{\hat{F}_{j+\frac{1}{2}} - \hat{F}_{j-\frac{1}{2}}}{h} = \left[-\frac{1}{3}\omega_{0,j-1/2}F_{j-3} + \left(\frac{7}{6}\omega_{0,j-1/2} + \frac{1}{3}\omega_{0,j+1/2} + \frac{1}{6}\omega_{1,j-1/2}\right)F_{j-2} \right.$$
$$+ \left(-\frac{11}{6}\omega_{0,j-1/2} - \frac{7}{6}\omega_{0,j+1/2} - \frac{5}{6}\omega_{1,j-1/2} - \frac{1}{6}\omega_{1,j+1/2} - \frac{1}{3}\omega_{2,j-1/2}\right)F_{j-1}$$
$$+ \left(\frac{11}{6}\omega_{0,j+1/2} - \frac{1}{3}\omega_{1,j-1/2} + \frac{5}{6}\omega_{1,j+1/2} - \frac{5}{6}\omega_{2,j-1/2} + \frac{1}{3}\omega_{2,j+1/2}\right)F_j$$
$$\left. + \left(\frac{1}{3}\omega_{1,j+1/2} + \frac{1}{6}\omega_{2,j-1/2} + \frac{5}{6}\omega_{2,j+1/2}\right)F_{j+1} - \frac{1}{6}\omega_{2,j+1/2}F_{j+2} \right] \Big/ h$$

By using the Taylor series expansion around j, the truncation error τ_{WENO} of the above equation is

$$\tau_{WENO} = \left(\frac{-\omega_{0,j-1/2} + \omega_{0,j+1/2} + \omega_{1,j-1/2} - \omega_{1,j+1/2}}{6} \right) h^2 \frac{\partial^3 F_j}{\partial x^3} +$$
$$+ \left(\frac{61\omega_{0,j-1/2} - 25\omega_{0,j+1/2} - 11\omega_{1,j-1/2} - \omega_{1,j+1/2} + \omega_{2,j-1/2} + 11\omega_{2,j+1/2}}{144} \right) h^3 \frac{\partial^4 F_j}{\partial x^4} +$$
$$+ \left(\frac{-91\omega_{0,j-1/2} + 19\omega_{0,j+1/2} + 9\omega_{1,j-1/2} - \omega_{1,j+1/2} - \omega_{2,j-1/2} + 9\omega_{2,j+1/2}}{240} \right) h^4 \frac{\partial^5 F_j}{\partial x^5} +$$
$$+ \left(\frac{1021\omega_{0,j-1/2} - 121\omega_{0,j+1/2} - 59\omega_{1,j-1/2} - \omega_{1,j+1/2} + \omega_{2,j-1/2} + 59\omega_{2,j+1/2}}{4320} \right) h^5 \frac{\partial^6 F_j}{\partial x^6} +$$
$$+ \left(\frac{-1163\omega_{0,j-1/2} + 83\omega_{0,j+1/2} + 41\omega_{1,j-1/2} - \omega_{1,j+1/2} - \omega_{2,j-1/2} + 41\omega_{2,j+1/2}}{10080} \right) h^6 \frac{\partial^7 F_j}{\partial x^7} + \quad (4.1)$$
$$+ \left(\frac{11341\omega_{0,j-1/2} - 505\omega_{0,j+1/2} - 251\omega_{1,j-1/2} - \omega_{1,j+1/2} + \omega_{2,j-1/2} + 251\omega_{2,j+1/2}}{241920} \right) h^7 \frac{\partial^8 F_j}{\partial x^8} +$$
$$+ \left(\frac{-11931\omega_{0,j-1/2} + 339\omega_{0,j+1/2} + 169\omega_{1,j-1/2} - \omega_{1,j+1/2} - \omega_{2,j-1/2} + 169\omega_{2,j+1/2}}{725760} \right) h^8 \frac{\partial^9 F_j}{\partial x^9} +$$
$$+ \left(\frac{110941\omega_{0,j-1/2} - 2041\omega_{0,j+1/2} - 1019\omega_{1,j-1/2} - \omega_{1,j+1/2} + \omega_{2,j-1/2} + 227\omega_{2,j+1/2}}{21772800} \right) h^9 \frac{\partial^{10} F_j}{\partial x^{10}} +$$
$$+ \ldots \quad .$$

From (4.1), we can determine the dissipation error and the dispersion error, which are respectively the even derivative terms and the odd derivative terms of τ_{WENO}:

Dissipation error:

$$E_{WENO,dissip} = \left(\frac{61\omega_{0,j-1/2} - 25\omega_{0,j+1/2} - 11\omega_{1,j-1/2} - \omega_{1,j+1/2} + \omega_{2,j-1/2} + 11\omega_{2,j+1/2}}{144} \right) h^3 \frac{\partial^4 F_j}{\partial x^4} +$$
$$+ \left(\frac{1021\omega_{0,j-1/2} - 121\omega_{0,j+1/2} - 59\omega_{1,j-1/2} - \omega_{1,j+1/2} + \omega_{2,j-1/2} + 59\omega_{2,j+1/2}}{4320} \right) h^5 \frac{\partial^6 F_j}{\partial x^6} +$$
$$+ \left(\frac{11341\omega_{0,j-1/2} - 505\omega_{0,j+1/2} - 251\omega_{1,j-1/2} - \omega_{1,j+1/2} + \omega_{2,j-1/2} + 251\omega_{2,j+1/2}}{241920} \right) h^7 \frac{\partial^8 F_j}{\partial x^8} + \quad (4.2)$$
$$+ \left(\frac{110941\omega_{0,j-1/2} - 2041\omega_{0,j+1/2} - 1019\omega_{1,j-1/2} - \omega_{1,j+1/2} + \omega_{2,j-1/2} + 227\omega_{2,j+1/2}}{21772800} \right) h^9 \frac{\partial^{10} F_j}{\partial x^{10}} +$$
$$+ \ldots$$

Dispersion error:

$$
\begin{aligned}
E_{WENO,disp} &= \left(\frac{-\omega_{0,j-1/2}+\omega_{0,j+1/2}+\omega_{1,j-1/2}-\omega_{1,j+1/2}}{6}\right)h^2\frac{\partial^3 F_j}{\partial x^3}+\\
&+\left(\frac{-91\omega_{0,j-1/2}+19\omega_{0,j+1/2}+9\omega_{1,j-1/2}-\omega_{1,j+1/2}-\omega_{2,j-1/2}+9\omega_{2,j+1/2}}{240}\right)h^4\frac{\partial^5 F_j}{\partial x^5}+\\
&+\left(\frac{-1163\omega_{0,j-1/2}+83\omega_{0,j+1/2}+41\omega_{1,j-1/2}-\omega_{1,j+1/2}-\omega_{2,j-1/2}+41\omega_{2,j+1/2}}{10080}\right)h^6\frac{\partial^7 F_j}{\partial x^7}+\\
&+\left(\frac{-11931\omega_{0,j-1/2}+339\omega_{0,j+1/2}+169\omega_{1,j-1/2}-\omega_{1,j+1/2}-\omega_{2,j-1/2}+169\omega_{2,j+1/2}}{725760}\right)h^8\frac{\partial^9 F_j}{\partial x^9}+\\
&+\ldots
\end{aligned}
\tag{4.3}
$$

On a similar analysis for the WCS, from equation (3.22),

$$
\begin{aligned}
&\left(-3\omega_{0,j-1/2}-\frac{3}{2}\omega_{1,j-1/2}-3\omega_{2,j-1/2}+3\omega_{0,j+1/2}+\frac{3}{2}\omega_{1,j+1/2}+3\omega_{2,j+1/2}\right)\frac{H'_{j+1/2}}{h}+\\
&+\left(2\omega_{0,j-1/2}+\frac{1}{4}\omega_{1,j-1/2}\right)F'_{j-1}+\\
&+\left(3\omega_{0,j-1/2}+\frac{5}{4}\omega_{1,j-1/2}+\omega_{2,j-1/2}-2\omega_{0,j+1/2}-\frac{1}{4}\omega_{1,j+1/2}\right)F'_{j}+\\
&+\left(\frac{1}{4}\omega_{1,j+1/2}+2\omega_{2,j+1/2}\right)F'_{j+1}\approx\\
&\approx\left[-\frac{1}{2}\omega_{0,j-1/2}F_{j-2}+\left(-\frac{5}{2}\omega_{0,j-1/2}-\frac{3}{4}\omega_{1,j-1/2}+\frac{1}{2}\omega_{0,j+1/2}\right)F_{j-1}+\right.\\
&+\left(-\frac{3}{4}\omega_{1,j-1/2}-\frac{5}{2}\omega_{2,j-1/2}+\frac{5}{2}\omega_{0,j+1/2}+\frac{3}{4}\omega_{1,j+1/2}\right)F_j+\\
&+\left(-\frac{1}{2}\omega_{2,j-1/2}+\frac{3}{4}\omega_{1,j+1/2}+\frac{5}{2}\omega_{2,j+1/2}\right)F_{j+1}+\\
&\left.+\frac{1}{2}\omega_{2,j+1/2}F_{j+2}\right]\Big/h
\end{aligned}
,
$$

by using the Taylor series expansion around *j*, the truncation error τ_{WCS} of the above equation is

$$
\begin{aligned}
\tau_{WCS} = &\left(\left(\omega_{0,j+1/2}-\omega_{0,j-1/2}\right)+\frac{1}{2}\left(\omega_{1,j+1/2}-\omega_{1,j-1/2}\right)+\left(\omega_{2,j+1/2}-\omega_{2,j-1/2}\right)\right)\frac{3}{h}\left(H'_{j+1/2}-F_j\right)+\\
&-\left(\left(\omega_{0,j+1/2}-\omega_{0,j-1/2}\right)+\frac{1}{2}\left(\omega_{1,j+1/2}-\omega_{1,j-1/2}\right)+\left(\omega_{2,j+1/2}-\omega_{2,j-1/2}\right)\right)\frac{3}{2}\frac{\partial F_j}{\partial x}+\\
&-\left(\left(\omega_{0,j+1/2}-\omega_{0,j-1/2}\right)+\frac{1}{2}\left(\omega_{1,j+1/2}-\omega_{1,j-1/2}\right)+\left(\omega_{2,j+1/2}-\omega_{2,j-1/2}\right)\right)\frac{h}{4}\frac{\partial^2 F_j}{\partial x^2}+\\
&+\left(\left(\omega_{0,j+1/2}-\omega_{0,j-1/2}\right)-\left(\omega_{2,j+1/2}-\omega_{2,j-1/2}\right)\right)\frac{h^2}{12}\frac{\partial^3 F_j}{\partial x^3}+\\
&+\left(5\omega_{0,j-1/2}-\omega_{0,j+1/2}-\frac{1}{2}\omega_{1,j-1/2}+\frac{1}{2}\omega_{1,j+1/2}+\omega_{2,j-1/2}-5\omega_{2,j+1/2}\right)\frac{h^3}{48}\frac{\partial^4 F_j}{\partial x^4}+\\
&+\left(-17\omega_{0,j-1/2}+\omega_{0,j+1/2}+\omega_{1,j-1/2}+\omega_{1,j+1/2}+\omega_{2,j-1/2}-17\omega_{2,j+1/2}\right)\frac{h^4}{240}\frac{\partial^5 F_j}{\partial x^5}+\\
&+\left(45\omega_{0,j-1/2}-\omega_{0,j+1/2}-\frac{3}{2}\omega_{1,j-1/2}+\frac{3}{2}\omega_{1,j+1/2}+\omega_{2,j-1/2}-45\omega_{2,j+1/2}\right)\frac{h^5}{1440}\frac{\partial^6 F_j}{\partial x^6}+\\
&+\left(-105\omega_{0,j-1/2}+\omega_{0,j+1/2}+2\omega_{1,j-1/2}+2\omega_{1,j+1/2}+\omega_{2,j-1/2}-105\omega_{2,j+1/2}\right)\frac{h^6}{10080}\frac{\partial^7 F_j}{\partial x^7}+\\
&+\left(229\omega_{0,j-1/2}-\omega_{0,j+1/2}-\frac{5}{2}\omega_{1,j-1/2}+\frac{5}{2}\omega_{1,j+1/2}+\omega_{2,j-1/2}-229\omega_{2,j+1/2}\right)\frac{h^7}{80640}\frac{\partial^8 F_j}{\partial x^8}+\\
&+\left(-481\omega_{0,j-1/2}+\omega_{0,j+1/2}+3\omega_{1,j-1/2}+3\omega_{1,j+1/2}+\omega_{2,j-1/2}-481\omega_{2,j+1/2}\right)\frac{h^8}{725760}\frac{\partial^9 F_j}{\partial x^9}+\\
&+\left(989\omega_{0,j-1/2}-\omega_{0,j+1/2}-\frac{7}{2}\omega_{1,j-1/2}+\frac{7}{2}\omega_{1,j+1/2}+\omega_{2,j-1/2}-989\omega_{2,j+1/2}\right)\frac{h^9}{7257600}\frac{\partial^{10} F_j}{\partial x^{10}}+\\
&+\left(-2009\omega_{0,j-1/2}+\omega_{0,j+1/2}+4\omega_{1,j-1/2}+4\omega_{1,j+1/2}+\omega_{2,j-1/2}-2009\omega_{2,j+1/2}\right)\frac{h^{10}}{79833600}\frac{\partial^{11} F_j}{\partial x^{11}}+\\
&+\ldots
\end{aligned}
\tag{4.4}
$$

Equation (4.4) is not purely dependent on the derivatives of F at j; it contains the derivative $H'_{j+1/2}$. To remove this dependence on H, an expansion on F around $j \pm 1/2$ needs to be considered.

To satisfy $F'_j = \dfrac{H'_{j+1/2}-H'_{j-1/2}}{h} = \dfrac{\hat{F}_{j+1/2}-\hat{F}_{j-1/2}}{h}$, we must have

$$
\hat{F}_{j\pm1/2} = F_{j\pm1/2} + \sum_{k=1}^{m-1} c_k h^{2k} \frac{\partial^{2k}}{\partial x^{2k}} F_{j\pm1/2} + O\left(h^{2m+1}\right),
$$

where c_k are constants.

For $m = 7$, for example,

$$c_1 = -\frac{1}{24};\quad c_2 = \frac{7}{5760};\quad c_3 = -\frac{31}{967680};$$
$$c_4 = \frac{127}{154828800};\quad c_5 = -\frac{73}{3503554560};\quad c_6 = \frac{1414477}{2678117105664000}.$$

By Taylor expansion around j,

$$\frac{H'_{j+1/2}}{h} = \frac{\hat{F}_{j+1/2}}{h} = \frac{F_j}{h} + \frac{1}{2}F'_j + \frac{h}{12}F''_j - \frac{h^3}{720}F_j^{(4)} + \frac{h^5}{30240}F_j^{(6)} - \frac{h^7}{1209600}F_j^{(8)} + \\ + \frac{31h^9}{743178240}F_j^{(10)} + O\left(h^{11}\right)$$

Since $\omega_{0,j\pm1/2} + \omega_{1,j\pm1/2} + \omega_{2,j\pm1/2} = 1$, the truncation error becomes

$$\begin{aligned}
\tau_{WCS} &= \left(-\omega_{0,j-1/2} + \omega_{2,j-1/2} + \omega_{0,j+1/2} - \omega_{2,j+1/2}\right)\frac{h^2}{12}\frac{\partial^3 F_j}{\partial x^3} + \\
&+ \left(5\omega_{0,j-1/2} - \frac{3}{5}\omega_{1,j-1/2} + \omega_{2,j-1/2} - \omega_{0,j+1/2} + \frac{3}{5}\omega_{1,j+1/2} - 5\omega_{2,j+1/2}\right)\frac{h^3}{48}\frac{\partial^4 F_j}{\partial x^4} + \\
&+ \left(-17\omega_{0,j-1/2} + \omega_{1,j-1/2} + \omega_{2,j-1/2} + \omega_{0,j+1/2} + \omega_{1,j+1/2} - 17\omega_{2,j+1/2}\right)\frac{h^4}{240}\frac{\partial^5 F_j}{\partial x^5} + \\
&+ \left(45\omega_{0,j-1/2} - \frac{10}{7}\omega_{1,j-1/2} + \omega_{2,j-1/2} - \omega_{0,j+1/2} + \frac{10}{7}\omega_{1,j+1/2} - 45\omega_{2,j+1/2}\right)\frac{h^5}{1440}\frac{\partial^6 F_j}{\partial x^6} + \\
&+ \left(-105\omega_{0,j-1/2} + 2\omega_{1,j-1/2} + \omega_{2,j-1/2} + \omega_{0,j+1/2} + 2\omega_{1,j+1/2} - 105\omega_{2,j+1/2}\right)\frac{h^6}{10080}\frac{\partial^7 F_j}{\partial x^7} + \\
&+ \left(229\omega_{0,j-1/2} - \frac{13}{5}\omega_{1,j-1/2} + \omega_{2,j-1/2} - \omega_{0,j+1/2} + \frac{13}{5}\omega_{1,j+1/2} - 229\omega_{2,j+1/2}\right)\frac{h^7}{80640}\frac{\partial^8 F_j}{\partial x^8} + \\
&+ \left(-481\omega_{0,j-1/2} + 3\omega_{1,j-1/2} + \omega_{2,j-1/2} + \omega_{0,j+1/2} + 3\omega_{1,j+1/2} - 481\omega_{2,j+1/2}\right)\frac{h^8}{725760}\frac{\partial^9 F_j}{\partial x^9} + \\
&+ \left(989\omega_{0,j-1/2} - \frac{36}{11}\omega_{1,j-1/2} + \omega_{2,j-1/2} - \omega_{0,j+1/2} + \frac{36}{11}\omega_{1,j+1/2} - 989\omega_{2,j+1/2}\right)\frac{h^9}{7257600}\frac{\partial^{10} F_j}{\partial x^{10}} + \\
&+ \left(-2009\omega_{0,j-1/2} + 4\omega_{1,j-1/2} + \omega_{2,j-1/2} + \omega_{0,j+1/2} + 4\omega_{1,j+1/2} - 2009\omega_{2,j+1/2}\right)\frac{h^{10}}{79833600}\frac{\partial^{11} F_j}{\partial x^{11}} + \\
&+ \ldots
\end{aligned} \tag{4.5}$$

From (4.5), we can determine the dissipation error and the dispersion error, which are respectively the even derivative terms and the odd derivative terms of τ_{WCS}:

Dissipation error:

$$E_{WCS,dissip} = \left(5\omega_{0,j-1/2} - \frac{3}{5}\omega_{1,j-1/2} + \omega_{2,j-1/2} - \omega_{0,j+1/2} + \frac{3}{5}\omega_{1,j+1/2} - 5\omega_{2,j+1/2}\right)\frac{h^3}{48}\frac{\partial^4 F_j}{\partial x^4} +$$
$$+\left(45\omega_{0,j-1/2} - \frac{10}{7}\omega_{1,j-1/2} + \omega_{2,j-1/2} - \omega_{0,j+1/2} + \frac{10}{7}\omega_{1,j+1/2} - 45\omega_{2,j+1/2}\right)\frac{h^5}{1440}\frac{\partial^6 F_j}{\partial x^6} +$$
$$+\left(229\omega_{0,j-1/2} - \frac{13}{5}\omega_{1,j-1/2} + \omega_{2,j-1/2} - \omega_{0,j+1/2} + \frac{13}{5}\omega_{1,j+1/2} - 229\omega_{2,j+1/2}\right)\frac{h^7}{80640}\frac{\partial^8 F_j}{\partial x^8} + \quad (4.6)$$
$$+\left(989\omega_{0,j-1/2} - \frac{36}{11}\omega_{1,j-1/2} + \omega_{2,j-1/2} - \omega_{0,j+1/2} + \frac{36}{11}\omega_{1,j+1/2} - 989\omega_{2,j+1/2}\right)\frac{h^9}{7257600}\frac{\partial^{10} F_j}{\partial x^{10}} +$$
$$+ \ldots$$

Dispersion error:

$$E_{WCS,disp} = \left(-\omega_{0,j-1/2} + \omega_{2,j-1/2} + \omega_{0,j+1/2} - \omega_{2,j+1/2}\right)\frac{h^2}{12}\frac{\partial^3 F_j}{\partial x^3} +$$
$$+\left(-17\omega_{0,j-1/2} + \omega_{1,j-1/2} + \omega_{2,j-1/2} + \omega_{0,j+1/2} + \omega_{1,j+1/2} - 17\omega_{2,j+1/2}\right)\frac{h^4}{240}\frac{\partial^5 F_j}{\partial x^5} +$$
$$+\left(-105\omega_{0,j-1/2} + 2\omega_{1,j-1/2} + \omega_{2,j-1/2} + \omega_{0,j+1/2} + 2\omega_{1,j+1/2} - 105\omega_{2,j+1/2}\right)\frac{h^6}{10080}\frac{\partial^7 F_j}{\partial x^7} + \quad (4.7)$$
$$+\left(-481\omega_{0,j-1/2} + 3\omega_{1,j-1/2} + \omega_{2,j-1/2} + \omega_{0,j+1/2} + 3\omega_{1,j+1/2} - 481\omega_{2,j+1/2}\right)\frac{h^8}{725760}\frac{\partial^9 F_j}{\partial x^9} +$$
$$+ \ldots$$

It is important to mention that the local truncation errors obtained in equations (4.1) and (4.5) are valid for any type of function. In the case of continuous smooth functions (e.g. sine wave), the values of the nonlinear weights $\omega_{0,j\pm1/2}$, $\omega_{1,j\pm1/2}$, and $\omega_{2,j\pm1/2}$ defined in (3.13) revert back to the optimal weights C_0, C_1 and C_2, respectively (WENO: C_0 = 1/10, C_1 = 6/10, C_2 = 3/10; WCS: C_0 = 1/18, C_1 = 8/9, C_2 = 1/18), since the values of the "smoothness" indicators $IS_{i,j\pm1/2}$, (i = 1,2,3) are the same. Then, the WCS and the WENO scheme achieve their highest possible order, 6th and 5th, respectively. In the case of a function with discontinuities, since the values of the "smoothness" indicators vary at regions near these discontinuities, the nonlinear weights differ from the optimal values, and so the order of the truncation errors of the schemes is reduced at these regions. The use of nonlinear weights in the calculations allows the

schemes to generate results with less oscillation near discontinuities, while keeping high order accuracy everywhere else.

In the following sections, these errors will be further analyzed, initially by a Fourier analysis (assuming a smooth continuous function, which should generate results similar to the linear weight schemes), and then near a shock, where the nonlinear weights will be used.

4.2 Fourier Analysis

A Fourier analysis of the errors associated with the WCS and WENO was performed by assuming that the spatial variable x is periodic over the domain [0, L], and $h = L / N$. By decomposing the F's into their Fourier coefficients (e.g., see [8] for details), the dissipation and dispersion errors can be analyzed through the plots of modified wavenumber versus wavenumber, as seen below (Figure 4.1). We notice that WCS is less dispersive than WENO, and has no dissipation (as a property of being a centered scheme).

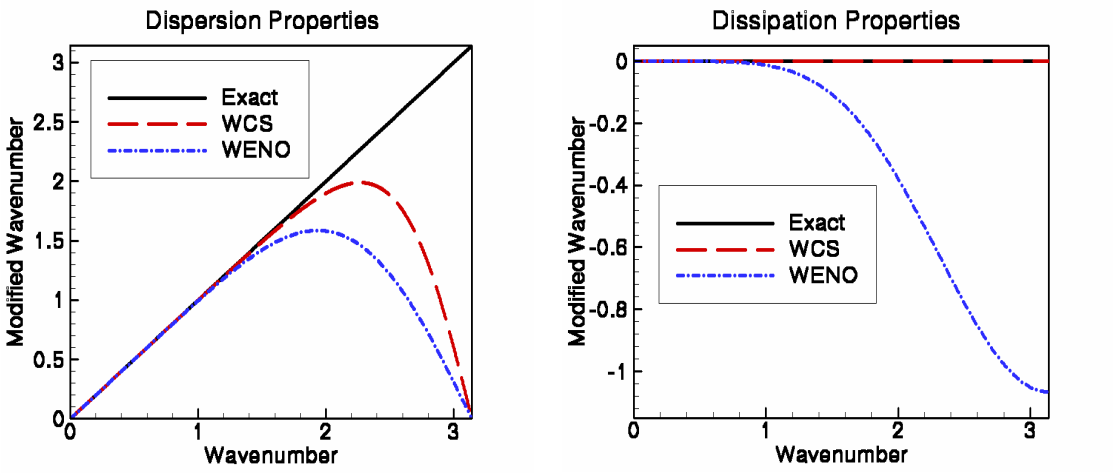

(a) (b)

Figure 4.1 (a) Dispersion and (b) dissipation relations for the WENO scheme and WCS

4.3 Analysis Near Shock

The results in the previous section are only applicable for continuous, smooth functions. Since the purpose of these numerical schemes is shock-capturing, then an analysis of the properties of the numerical schemes near a shock is necessary.

In a similar study as in [6], the weights $\omega_{0,j+1/2}, \omega_{1,j+1/2}$, and $\omega_{2,j+1/2}$ of WENO and WCS are calculated for the function

$$f(x_j) = \begin{cases} \sin(2\pi x_j), & 0 \le x_j \le 0.5 \\ 1 - \sin(2\pi x_j), & 0.5 < x_j \le 1 \end{cases},$$

(Figure 4.2), where $x_j = j\Delta x$ and $\Delta x = \frac{1}{40}$.

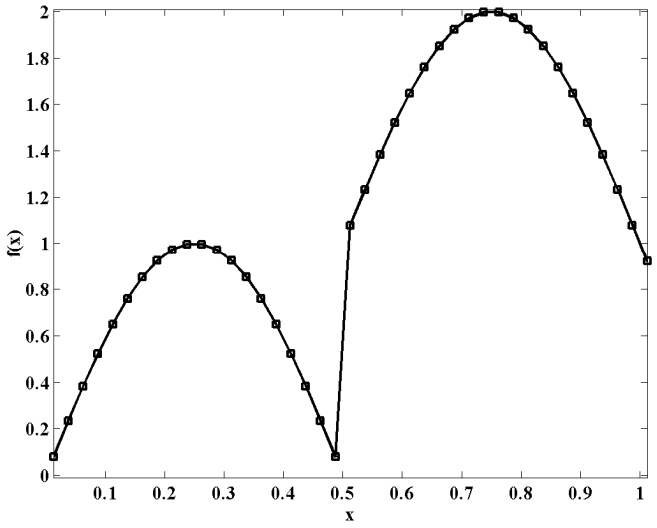

Figure 4.2 Function *f*(*x*), with 40 divisions

In Figure 4.3, the weights $\omega_{0,j+1/2}, \omega_{1,j+1/2}$ and $\omega_{2,j+1/2}$ are shown for WENO and WCS. Both schemes show similar behavior due to using the same smoothness indicators. We observe that near critical points (*x* = 0.25 and 0.75), the weights are not optimal (a small shift occurs) and so the numerical schemes do not achieve their maximum orders at those points.

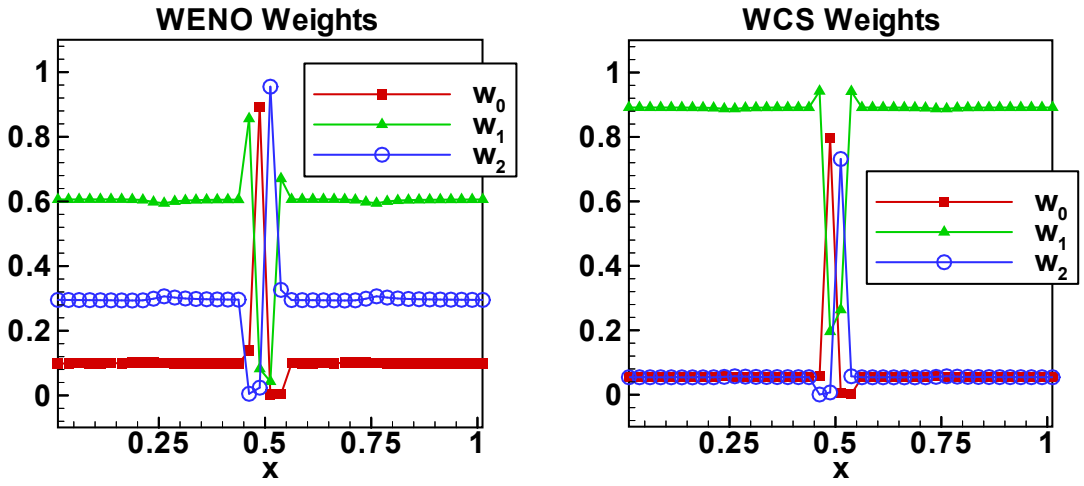

Figure 4.3 (a) WENO and (b) WCS weights calculated using $f(x)$. $w_i = \omega_{i,j+1/2}$, $i = 0,1,2$.

Also, near the discontinuity at $x = 0.5$, the weight $\omega_{0,18+1/2}$ (left of the discontinuity) for the WCS is very close to the optimal value C_0, which is not observed for the WENO scheme.

Now, let us observe the behavior of the truncation errors near a shock. We consider, as worst cases, when only one of the stencils E_0, E_1, or E_2 does not include a discontinuity, that is, only one of the weights is different than zero. Let us analyze three cases. For each case, the truncation errors τ_{WENO}, equation (4.1), and τ_{WCS}, equation (4.5), are calculated with the given values for the weights:

1. $\omega_{0,j\pm1/2} = 1;\ \omega_{1,j\pm1/2} = 0;\ \omega_{2,j\pm1/2} = 0$:

$$\tau_{WENO} = \frac{h^3}{4}\frac{\partial^4 F_j}{\partial x^4} + \frac{3h^4}{10}\frac{\partial^5 F_j}{\partial x^5} - \frac{5h^5}{24}\frac{\partial^6 F_j}{\partial x^6} + \frac{3h^6}{28}\frac{\partial^7 F_j}{\partial x^7} - \frac{43h^7}{960}\frac{\partial^8 F_j}{\partial x^8} + O\left(h^8\right)$$

$$\tau_{WCS} = \frac{h^3}{12}\frac{\partial^4 F_j}{\partial x^4} - \frac{h^4}{15}\frac{\partial^5 F_j}{\partial x^5} + \frac{11h^5}{360}\frac{\partial^6 F_j}{\partial x^6} - \frac{13h^6}{1260}\frac{\partial^7 F_j}{\partial x^7} + \frac{19h^7}{6720}F_j^{(8)} + O\left(h^8\right)$$

2. $\omega_{0,j\pm1/2}=0;\ \omega_{1,j\pm1/2}=1;\ \omega_{2,j\pm1/2}=0:$

$$\tau_{WENO}=-\frac{h^3}{12}\frac{\partial^4 F_j}{\partial x^4}-\frac{h^4}{30}\frac{\partial^5 F_j}{\partial x^5}+\frac{h^5}{72}\frac{\partial^6 F_j}{\partial x^6}-\frac{h^6}{252}\frac{\partial^7 F_j}{\partial x^7}+\frac{h^7}{960}\frac{\partial^8 F_j}{\partial x^8}+O\left(h^8\right)$$

$$\tau_{WCS}=\frac{h^4}{120}\frac{\partial^5 F_j}{\partial x^5}+\frac{h^6}{2520}\frac{\partial^7 F_j}{\partial x^7}+O\left(h^8\right)$$

3. $\omega_{0,j\pm1/2}=0;\ \omega_{1,j\pm1/2}=0;\ \omega_{2,j\pm1/2}=1:$

$$\tau_{WENO}=\frac{h^3}{12}\frac{\partial^4 F_j}{\partial x^4}-\frac{h^4}{30}\frac{\partial^5 F_j}{\partial x^5}-\frac{h^5}{72}\frac{\partial^6 F_j}{\partial x^6}-\frac{h^6}{252}\frac{\partial^7 F_j}{\partial x^7}-\frac{h^7}{960}\frac{\partial^8 F_j}{\partial x^8}+O\left(h^8\right)$$

$$\tau_{WCS}=-\frac{h^3}{12}\frac{\partial^4 F_j}{\partial x^4}-\frac{h^4}{15}\frac{\partial^5 F_j}{\partial x^5}-\frac{11h^5}{360}\frac{\partial^6 F_j}{\partial x^6}-\frac{13h^6}{1260}\frac{\partial^7 F_j}{\partial x^7}-\frac{19h^7}{6720}\frac{\partial^8 F_j}{\partial x^8}+O\left(h^8\right)$$

We observe that for all three cases, the truncation error for WCS is similar or better than the truncation error for WENO. We can also observe that WCS is best when the central stencil is used (case 2). In this case, WCS is an order higher than WENO, and it is only dispersive (has no dissipation terms).

In the next Chapter, we will show numerical results obtained by each scheme separately, and that a new scheme with a linear combination of WENO scheme and WCS shows improved results.

CHAPTER 5

THE MODIFIED WEIGHTED COMPACT SCHEME

In this Chapter, we will show, by numerical examples, that a linear combination of the WENO scheme and WCS generates better results in one-dimensional cases than each scheme individually.

5.1 One-Dimensional Numerical Examples

We have seen that the Weighted Compact Scheme has no dissipation and has a lower dispersion than WENO in smooth areas and that, near discontinuities, it has lower truncation errors (Chapter 4). This would indicate that it would be ideal for shock-capturing and high resolution of small length scales. Unfortunately, the absence of dissipation in smooth areas causes non-physical oscillations generated around the shock not to be dissipated, and in many cases, to increase without bounds. The WENO scheme, on the other hand, contains too much dissipation and can miss small details. This will be demonstrated through one-dimensional numerical examples.

The governing equations are the 1D Euler equations

$$\frac{\partial \boldsymbol{q}}{\partial t} + \frac{\partial \boldsymbol{F}}{\partial x} = 0\,, \tag{5.1}$$

with

$$\boldsymbol{q} = \left[\rho, \rho u, E\right]^T; \quad \boldsymbol{F} = \left[\rho u, \rho u^2 + p, u(E+p)\right]^T\,,$$

where the three-step TVD Runge-Kutta scheme is used in time marching and the Lax-Friedrich flux vector splitting is used to define $\boldsymbol{F}^+$ and $\boldsymbol{F}^-$. The derivatives of the fluxes are determined by either WENO or WCS.

Let us consider, first, the shock-tube problem. With initial conditions

$$[\rho,u,p]=\begin{cases}[1,0,1], & \text{if } x<0\\ [0.125,0,0.1], & \text{if } x\geq 0\end{cases}, \tag{5.2}$$

the Euler equations are solved until time t = 2. A comparison of the solution of (5.1) with initial conditions (5.2) with the WENO scheme and with WCS using N = 100 grid spaces is performed with the WENO scheme using N = 1600 grid spaces (which we consider an approximation to the exact solution) in Figure (5.1). We observe that, as described previously, the WCS generates non-physical oscillations in the smooth regions, while the WENO scheme has too much dissipation in smooth regions.

Another example is the shock-entropy wave interaction. In this case, the 1D Euler equations (5.1) are solved with initial conditions

$$[\rho,u,p]=\begin{cases}[3.857143,2.629369,10.33333], & \text{if } x<-4\\ [1+0.2\sin(5x),0,1], & \text{if } x\geq -4\end{cases}, \tag{5.3}$$

until time t = 1.8. A comparison of the WENO scheme with N = 200 and with N = 1600 grid spaces is shown in Figure (5.2). This shows that the WENO scheme misses small details in areas of high frequency waves. The WCS cannot generate comparable results since non-physical oscillations increase without bounds.

5.2 The New Scheme

Based on the results of the last section, we will consider a linear combination of the WCS and of the WENO scheme, which constructs a new scheme we call the Modified Weighted Compact Scheme (MWCS). Let α be a constant. Then, the flux of the MWCS, $\hat{F}_{MWCS}$, is given by

$$\hat{F}_{MWCS}=\alpha\hat{F}_{WCS}+(1-\alpha)\hat{F}_{WENO}, \tag{5.4}$$

where $\hat{F}_{WCS}$ is the numerical flux for WCS and $\hat{F}_{WENO}$ is the numerical flux for WENO. WCS is recovered when $\alpha=1$ and WENO is recovered when $\alpha=0$.

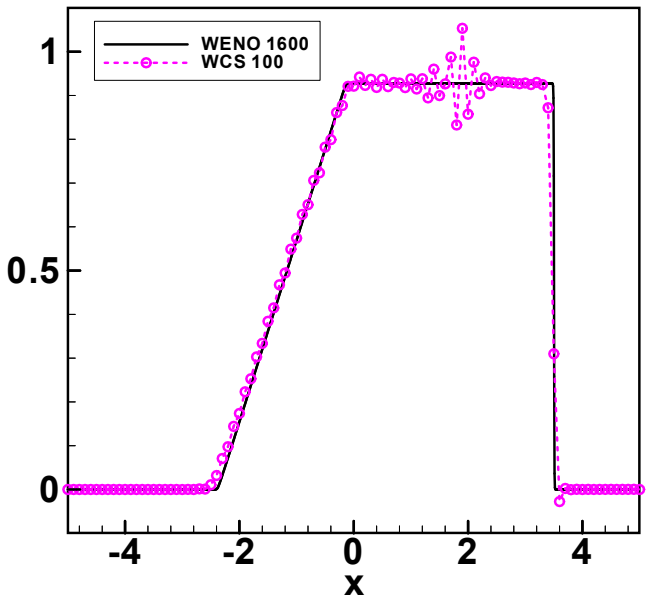

(a)

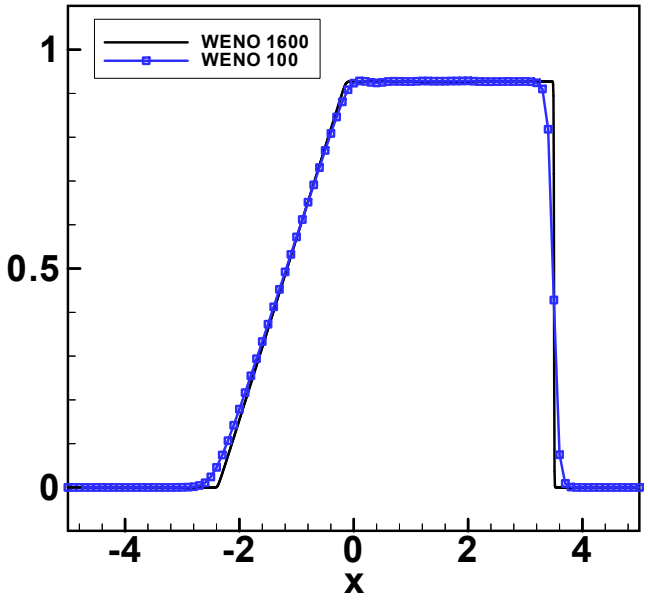

(b)

Figure 5.1 (a) WCS and (b) WENO solutions to the shock tube problem, $t = 2$.

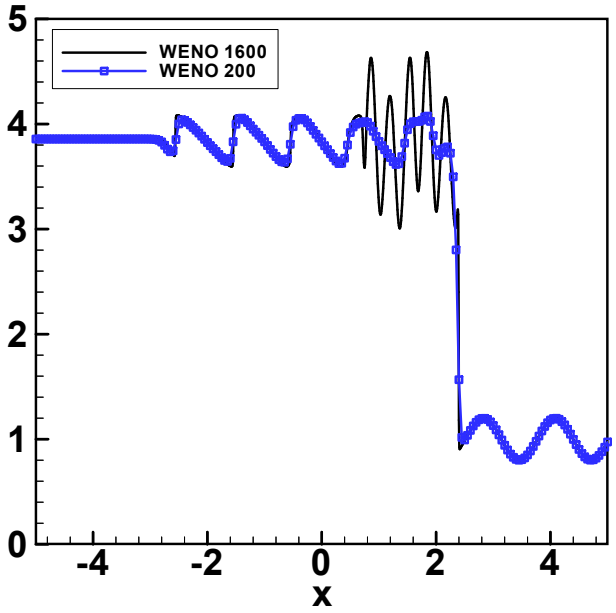

Figure 5.2 WENO solution to the shock-entropy wave interaction problem, t = 1.8.

From numerical observation, an optimized value of $\alpha = 0.72$ gives the best solution without oscillation. A comparison of the MWCS and the WENO scheme for the 1D Euler equations with initial conditions (5.2) and (5.3) is shown in Figures (5.3) and (5.4), respectively.

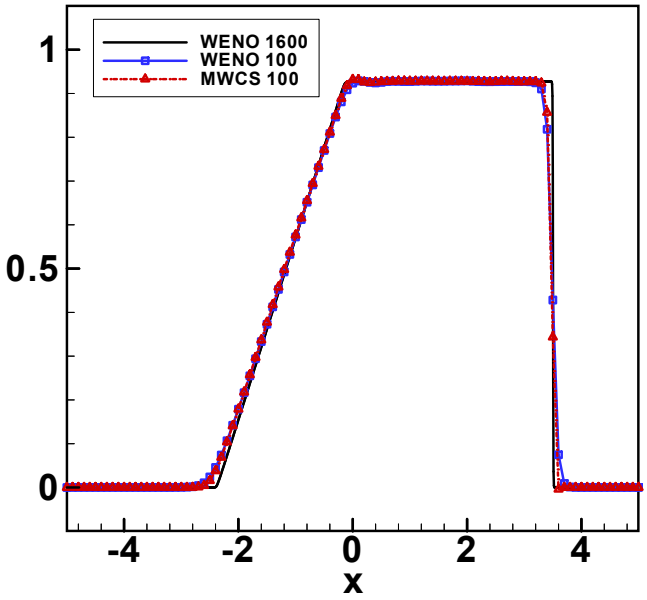

Figure 5.3 MWCS and WENO solutions to the shock tube problem, $t = 2$, $N = 100$.

These results show that the MWCS improves the results obtained by the WENO scheme alone, and does not generate spurious oscillations in one-dimensional cases. Unfortunately, for two- and three-dimensional cases, tests show that, without the application of filters, stable results cannot be achieved. This implies that the combination WCS-WENO is not ideal for higher dimensional cases, but the combination of a high-resolution scheme for smooth regions and a biased shock-capturing scheme for shock areas is promising, as long as the high-resolution scheme contains a small amount of dissipation and the schemes are applied at proper locations by the use of a shock/discontinuity detector.

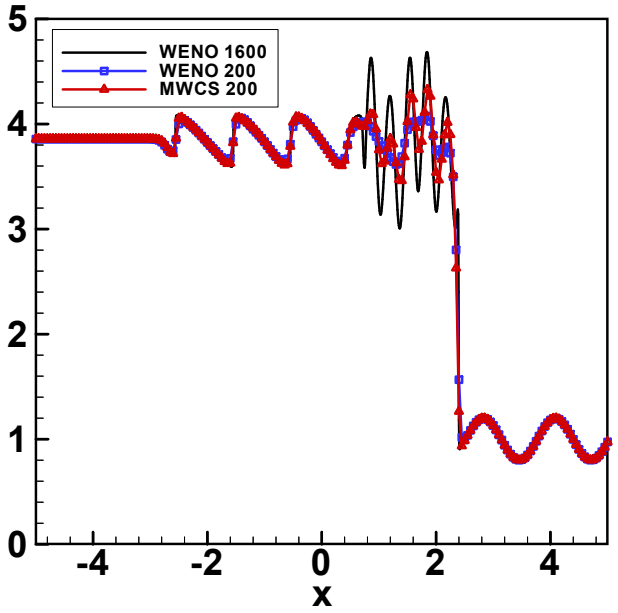

(a)

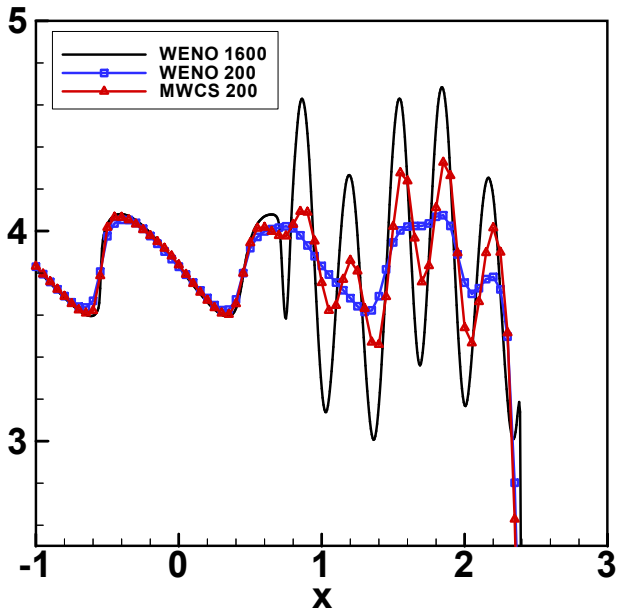

(b)

Figure 5.4 (a) MWCS and WENO solutions to the shock-entropy wave interaction problem and (b) a locally enlarged view; t = 1.8, N = 200.

CHAPTER 6

THE TWO-STEP SHOCK/DISCONTINUITY DETECTOR

Based on the results of the previous Chapter, it is clear that the use of a combination of numerical schemes greatly improves the results of capturing small scale features and the shock. However, an effective shock detector is essential for the success of the combined scheme. In this Chapter, we will describe the new Two-Step shock/discontinuity detector and show its effectiveness through numerical examples, comparing with two popular switches/detectors: the Harten switch [4], and the WENO weights, portrayed in equation (3.13).

6.1 The Harten Switch Function and the WENO Weights

The Harten switch [4] is an automatic switch function that is capable of detecting large changes in the variation of function values f_i. It generates values between 0 and 1, where lower values indicate smoothness and higher values indicate non-smoothness. It is defined by

$$\theta_{i+1/2} = \max\left(\hat{\theta}_i, \hat{\theta}_{i+1}\right), \tag{6.1}$$

where

$$\hat{\theta}_i = \begin{cases} \left| \dfrac{|\Delta f_{i+1/2}| - |\Delta f_{i-1/2}|}{|\Delta f_{i+1/2}| + |\Delta f_{i-1/2}|} \right|^p, & \text{if } |\Delta f_{i+1/2}| + |\Delta f_{i-1/2}| > \varepsilon, \\ 0, & \text{otherwise} \end{cases} \tag{6.2}$$

with $\Delta f_{i+1/2} = f_{i+1} - f_i$, ε as a suitably chosen measure of insignificant variation in f, and p is a constant taken generally as 1.

The WENO weights [6] (3.13) use smoothness indicators $IS_{i,j+1/2}, i = 0,1,2$, defined in (3.14) to determine changes in the variation of function values f_i. If we assume that all weights

have equal contribution, a function is considered smooth if all weights are approximately 1/3. The weights are redefined as

$$\omega_{i,j+1/2} = \frac{\alpha_{i,j+1/2}}{\sum_{k=0}^{2} \alpha_{k,j+1/2}}; \quad \alpha_{i,j+1/2} = \frac{1}{\left(\varepsilon + IS_{i,j+1/2}\right)^{p}}, \quad i = 0,1,2 . \tag{6.3}$$

6.2 The Two-Step Detector

As the name implies, there are two main steps in this shock/discontinuity detector. Let us assume that function values $f(x_i) = f_i$, $I = 1,2,\ldots,N$ are given on a uniform grid, with $x_{i+1} - x_i = h$.

Step 1: Determine the multigrid ratio of the approximation of the sum of the fourth, fifth and sixth truncation error terms for $F = f + A\sin(k\pi x + \phi)$, where A is a small number, and select the points where the ratio is smaller than 4. The multigrid truncation error ratio check is given by

$$MR(i,h) = \frac{T_C(i,h)}{T_F(i,h) + \varepsilon}, \tag{6.4}$$

where ε is a small number to avoid division by zero and $T_F(i,h)$ and $T_C(i,h)$ are the approximation of the sum of the fourth, fifth and sixth truncation error terms for the fine grid of spacing h and for the coarse grid of spacing $2h$, respectively, at the same position x_i. They are defined as

$$T_F(i,h) = \frac{h^4}{4!}\frac{\partial^4 F(x_i)}{\partial x^4} + \frac{h^5}{5!}\frac{\partial^5 F(x_i)}{\partial x^5} + \frac{h^6}{6!}\frac{\partial^6 F(x_i)}{\partial x^6}; \tag{6.5}$$

$$T_C(i,h) = \frac{(2h)^4}{4!}\frac{\partial^4 F(x_i)}{\partial x^4} + \frac{(2h)^5}{5!}\frac{\partial^5 F(x_i)}{\partial x^5} + \frac{(2h)^6}{6!}\frac{\partial^6 F(x_i)}{\partial x^6}.$$

Then, the multigrid ratio value $MR(i,h)$ is at least 16 for smooth regions and close to 1 in non-smooth regions. Because the derivatives are calculated numerically by the sixth-order compact scheme [8], we use a cutoff value of 4. Therefore, any point that has a value greater

or equal than 4 passes the test and is considered smooth. Otherwise, the point is picked out for the second left- and right-hand slope ratio check.

Step 2: Calculate the local left- and right-slope ratio check only at the points that have a multigrid ratio less than 4, and use a cutoff value of 0.8 to define a 0/1 switch function.

The local slope ratio check is defined by

$$LR(i) = \left| \frac{\left|\frac{f'_R(i)}{f'_L(i)}\right| - \left|\frac{f'_L(i)}{f'_R(i)}\right|}{\left|\frac{f'_R(i)}{f'_L(i)}\right| + \left|\frac{f'_L(i)}{f'_R(i)}\right| + \varepsilon} \right| = \left| \frac{[f'_R(i)]^2 - [f'_L(i)]^2}{[f'_R(i)]^2 + [f'_L(i)]^2 + \varepsilon} \right|, \tag{6.6}$$

where ε is a small number to avoid division by zero, $f'_L(i) = 3f_i - 4f_{i-1} + f_{i-2}$ and $f'_R(i) = 3f_i - 4f_{i+1} + f_{i+2}$. We notice that the definition of $LR(i)$ is similar to the Harten switch function (6.2), but the higher order approximation of the left- and right-hand slopes and the use of the square of the slopes greatly improve the detection.

The application of the compact scheme for the calculation of the derivatives on the first check gives a relatively inexpensive cost for the Two-Step detector. To guarantee a universal formulation, a normalized data set $\bar{f}_i, i = 1,...,N$ is used during the two-step check, with

$$\bar{f}_i = \frac{f_i - f_{\min}}{|f_{\max} - f_{\min}|}, \tag{6.7}$$

where $f_{\max}$ and $f_{\min}$ are respectively the maximum and minimum values of the original data set. This new shock detector is capable of detecting discontinuities in the function and also in the first, second and third derivatives of any function. Let us show the efficacy of the Two-Step detector with numerical examples.

6.3 Computational Results

With eight different examples, we will compare the Two-Step detector with the Harten switch function (6.1) and the modified WENO weights (6.3). The Two-Step detector equals zero

and the Harten switch function is approximately zero, while the WENO weights are approximately equal to 1/3, in smooth regions.

6.3.1 Example 1: Jump function

The function is defined as

$$f(x)=\begin{cases}0, & \text{if } -1\le x\le 0\\ 1, & \text{if } 0<x\le 1\end{cases},\ N=81 \text{ points.} \tag{6.8}$$

Figure (6.1) shows that all three shock detectors perform very well and accurately detect the discontinuity in the function.

6.3.2 Example 2: Jump slope

For this example, the function is defined as

$$f(x)=\begin{cases}1+x, & \text{if } -1\le x\le 0\\ 1, & \text{if } 0<x\le 1\end{cases},\ N=81 \text{ points.} \tag{6.9}$$

Figure (6.2) shows that the first derivative discontinuity is accurately detected by Two-Step, Harten and WENO weights.

6.3.3 Example 3: High-frequency sound waves (eight points per wave)

The function is defined by

$$f(x)=\sin\left[\frac{(N-1)\pi x}{8}\right],\ -1\le x\le 1,\ N=81 \text{ points.} \tag{6.10}$$

The high frequency sound waves with eight grid points per wave results show that both Harten and WENO treat the sound waves as non-smooth, while the Two-Step detector correctly indicates them as smooth (Figure 6.3).

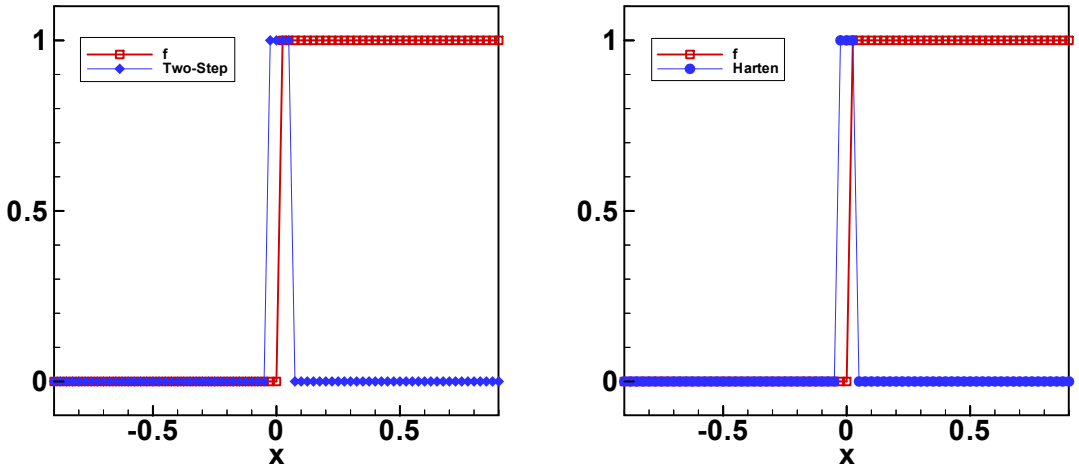

(a)

(b)

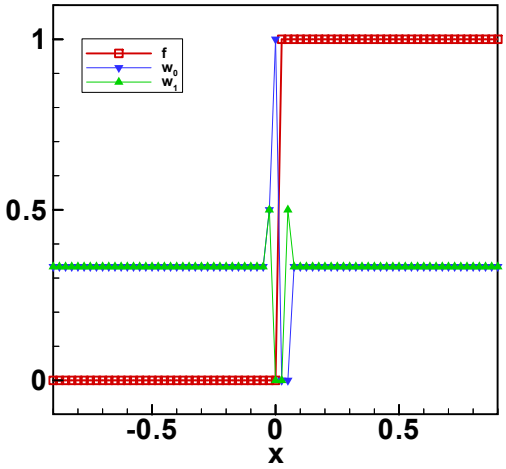

(c)

Figure 6.1 Shock detector for jump function: (a) Two-step (b) Harten (c) WENO. $w_i = \omega_{i,j+1/2}, i = 0,1.$

6.3.4 Example 4: Mixed high-frequency sound waves

The combination of two high-frequency sound waves, with 7 and with 9 grid points per wave, generates a more intriguing case, where the function is defined by

$$f(x) = \sin\left[\frac{(N-1)\pi x}{7}\right] + \sin\left[\frac{(N-1)\pi x}{9}\right], \quad -1 \le x \le 1, \ N = 81 \text{ points.} \tag{6.11}$$

As in the previous example, Harten and WENO cannot identify the function as smooth, while the Two-Step detector successfully detects all points as smooth (Figure 6.4).

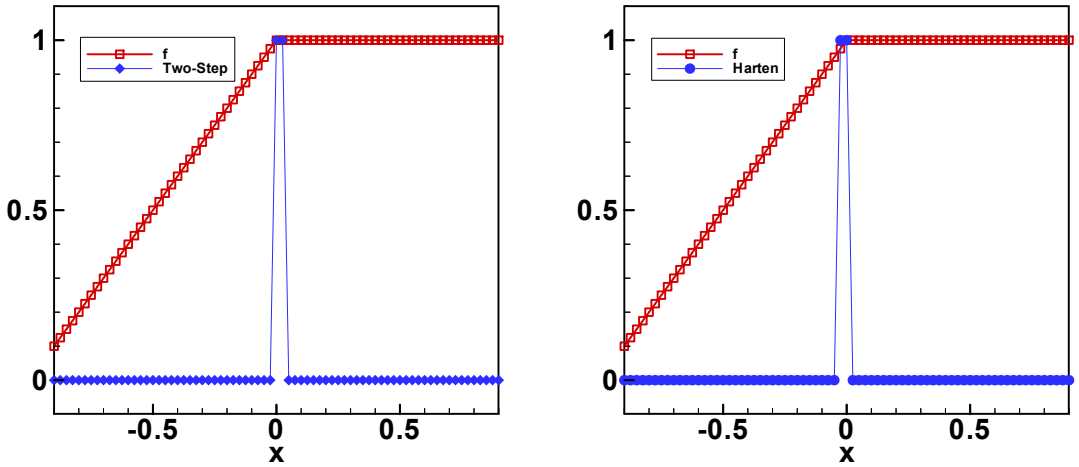

(a)

(b)

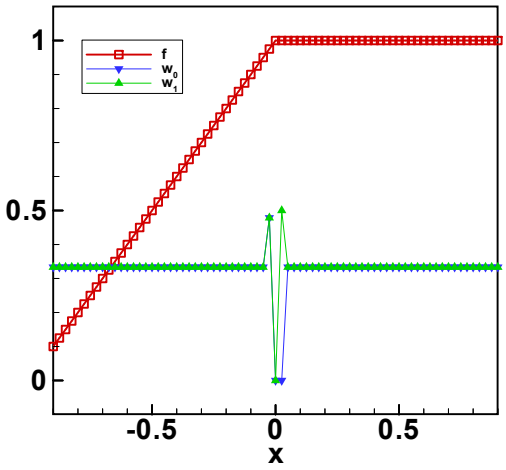

(c)

Figure 6.2 Shock detector for jump slope function: (a) Two-step (b) Harten (c) WENO. $w_i = \omega_{i,j+1/2}, i = 0,1.$

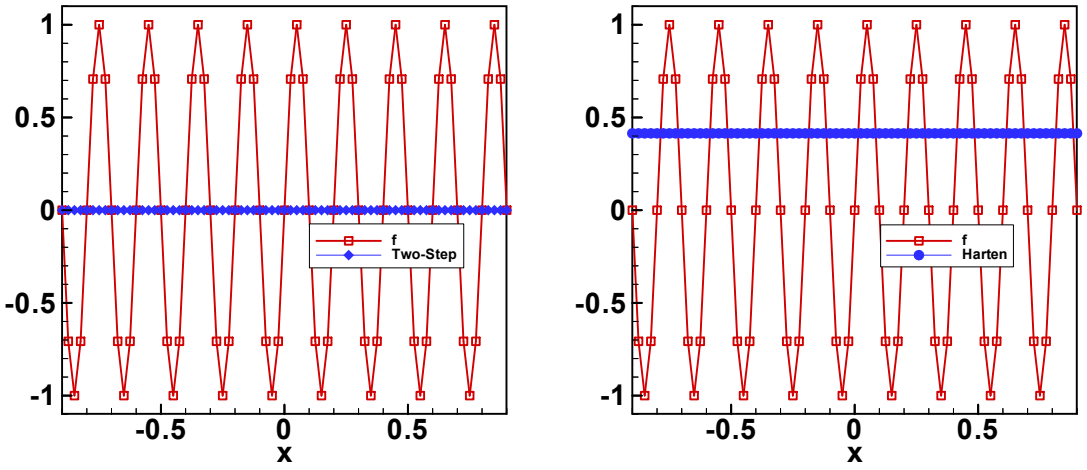

(a)

(b)

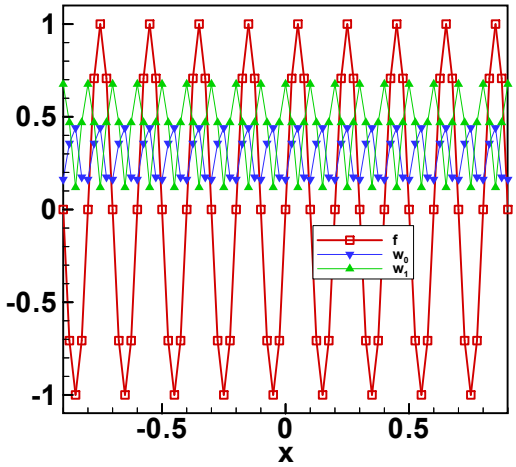

(c)

Figure 6.3 Shock detector for high-frequency sound waves: (a) Two-step (b) Harten (c) WENO. $w_i = \omega_{i,j+1/2}, i = 0,1.$

6.3.5 Example 5: Smooth function with a large slope

A smooth exponential function with a large slope, as defined by

$$f(x) = \exp\left(-300x^2\right), \quad -1 \le x \le 1, \ N = 81 \text{ points}, \tag{6.12}$$

is mistakenly treated by Harten and WENO as non-smooth, but Two-Step can correctly detect it as smooth (Figure 6.5).

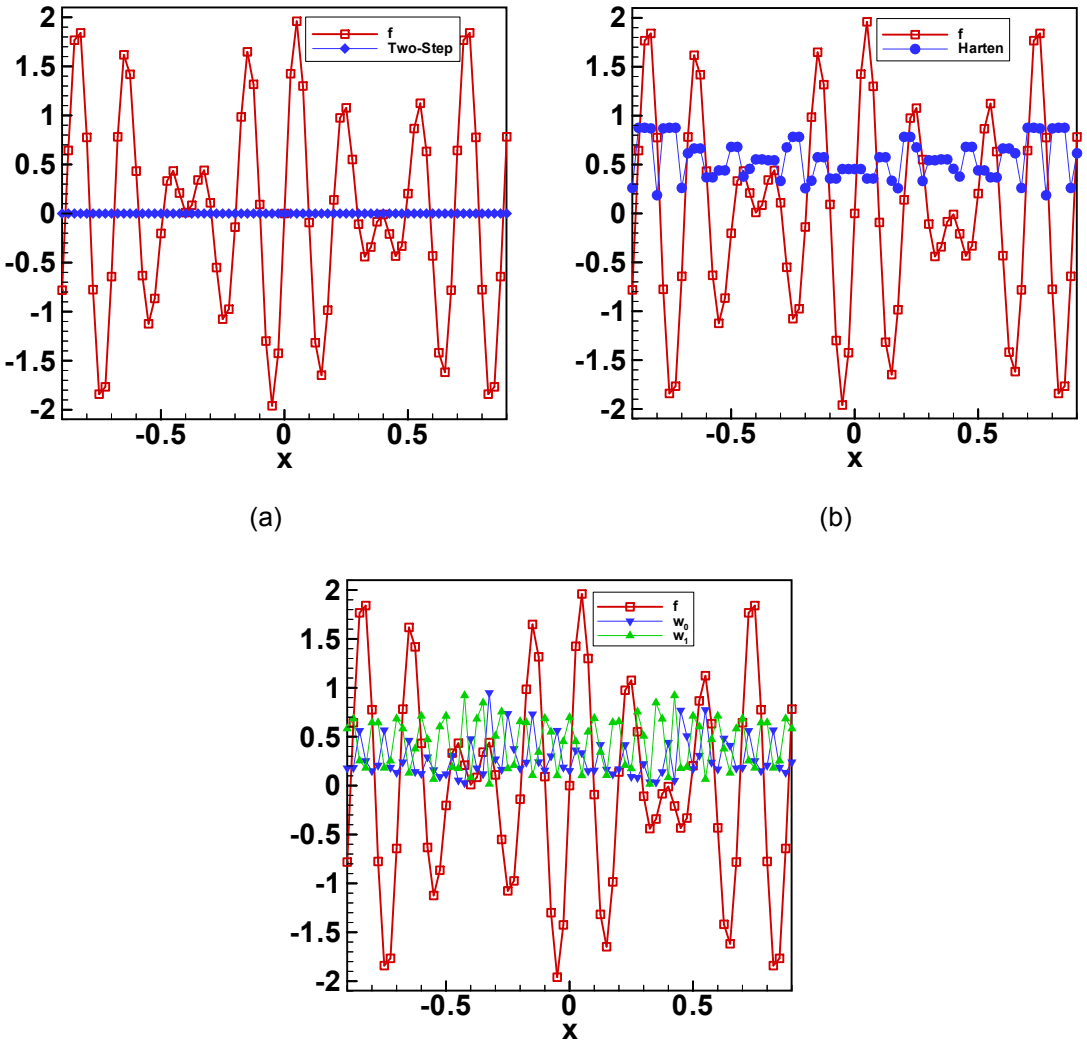

(a) (b)

(c)

Figure 6.4 Shock detector for mixed high-frequency sound waves: (a) Two-step (b) Harten (c) WENO. $w_i = \omega_{i,j+1/2}, i = 0,1.$

6.3.6 Example 6: Smooth function with large slope and jumps in slope

The function defined by

$$f(x)=\begin{cases}\sqrt{1-\left(\frac{10}{3}x\right)^2}, & \text{if } -\frac{3}{10}\le x\le\frac{3}{10},\ N=81 \text{ points}\\ 0, & \text{otherwise}\end{cases} \tag{6.13}$$

is smooth in the central part, but contains discontinuities in the derivative. As with other examples, Harten mistreats the critical point at $x = 0$ as non-smooth, while WENO has trouble with the large slopes. In contrast, Two-Step correctly identifies only the discontinuities in the derivative (Figure 6.6).

6.3.7 Example 7: 1D Shock-Entropy Wave Interaction

To test the capabilities of the new shock detector in more complex cases, we apply it to the one-dimensional problem of the shock-entropy wave interaction. The 1D Euler equations (5.1) are solved with initial conditions (5.3) to time $t = 1.8$ with $N = 201$ points. All three detectors identify the shocks (including weak shocks), but Harten and WENO treat the sound waves as non-smooth (Figure 6.7). This is why WENO smears the sound wave if the grid is not fine enough.

6.3.8 Example 8: 1D Shock Tube Problem

The one-dimensional shock tube problem is also tested. The 1D Euler equations (5.1) are solved with initial conditions (5.2) to time $t = 2.0$ with $N = 101$ points. Again, all three detectors identify the shock, but Harten and WENO also detect the expansion wave as non-smooth (Figure 6.8). This causes the expansion wave to be smeared by WENO.

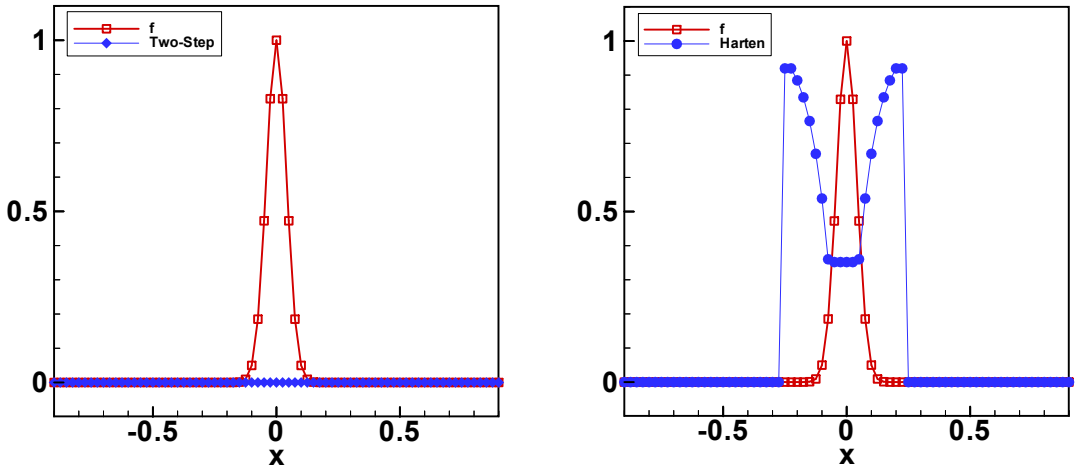

(a)

(b)

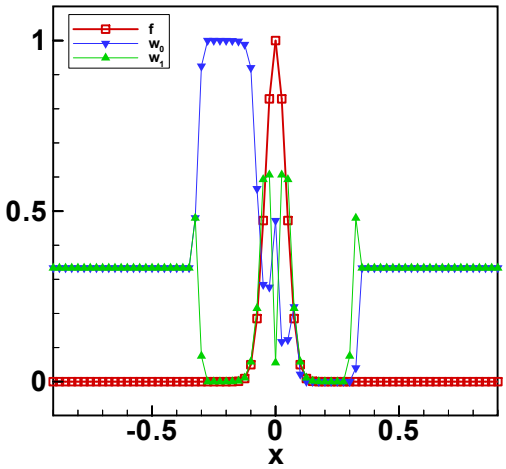

(c)

Figure 6.5 Shock detector for smooth function with a large slope: (a) Two-step (b) Harten (c) WENO. $w_i = \omega_{i,j+1/2}, i = 0,1.$

6.4 Proposal of New Scheme Formulation with Shock Detector

As mentioned in the last chapter, a new scheme F may be developed with the application of the Two-Step detector switch α by combining a low dissipation, high-resolution scheme F_1 for the smooth region with a bias upwind scheme F_2 for the shock region, where

$$F = (1-\alpha)F_1 + \alpha F_2 . \tag{6.14}$$

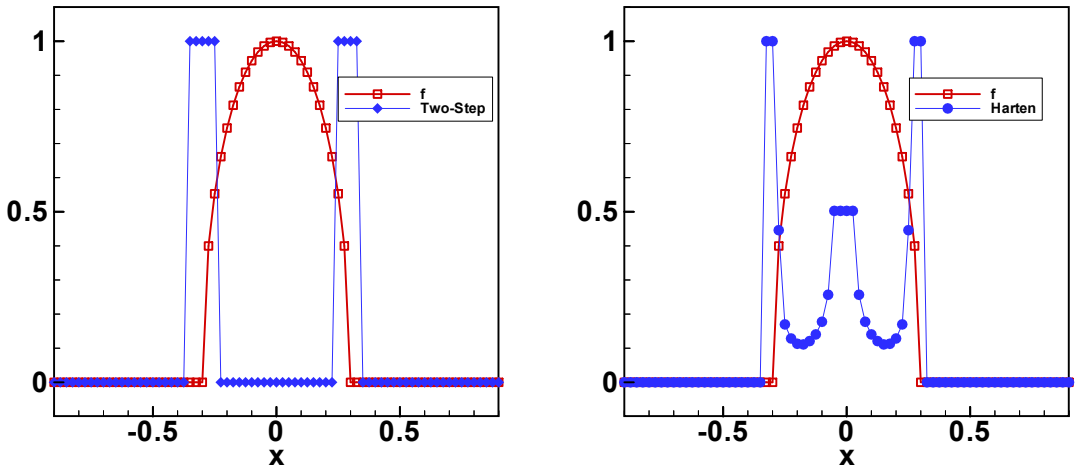

(a)

(b)

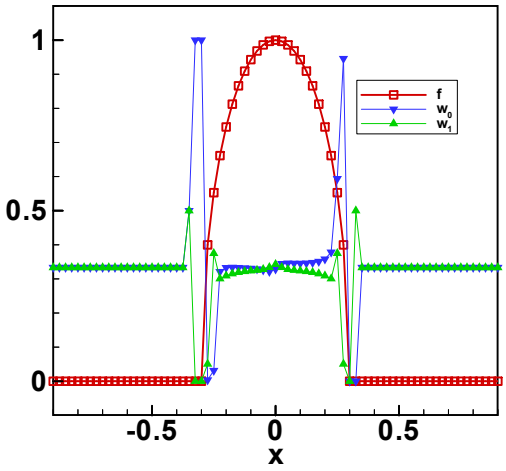

(c)

Figure 6.6 Shock detector for large slope and jump in slope: (a) Two-step (b) Harten (c) WENO. $w_i = \omega_{i,j+1/2}, i = 0,1.$

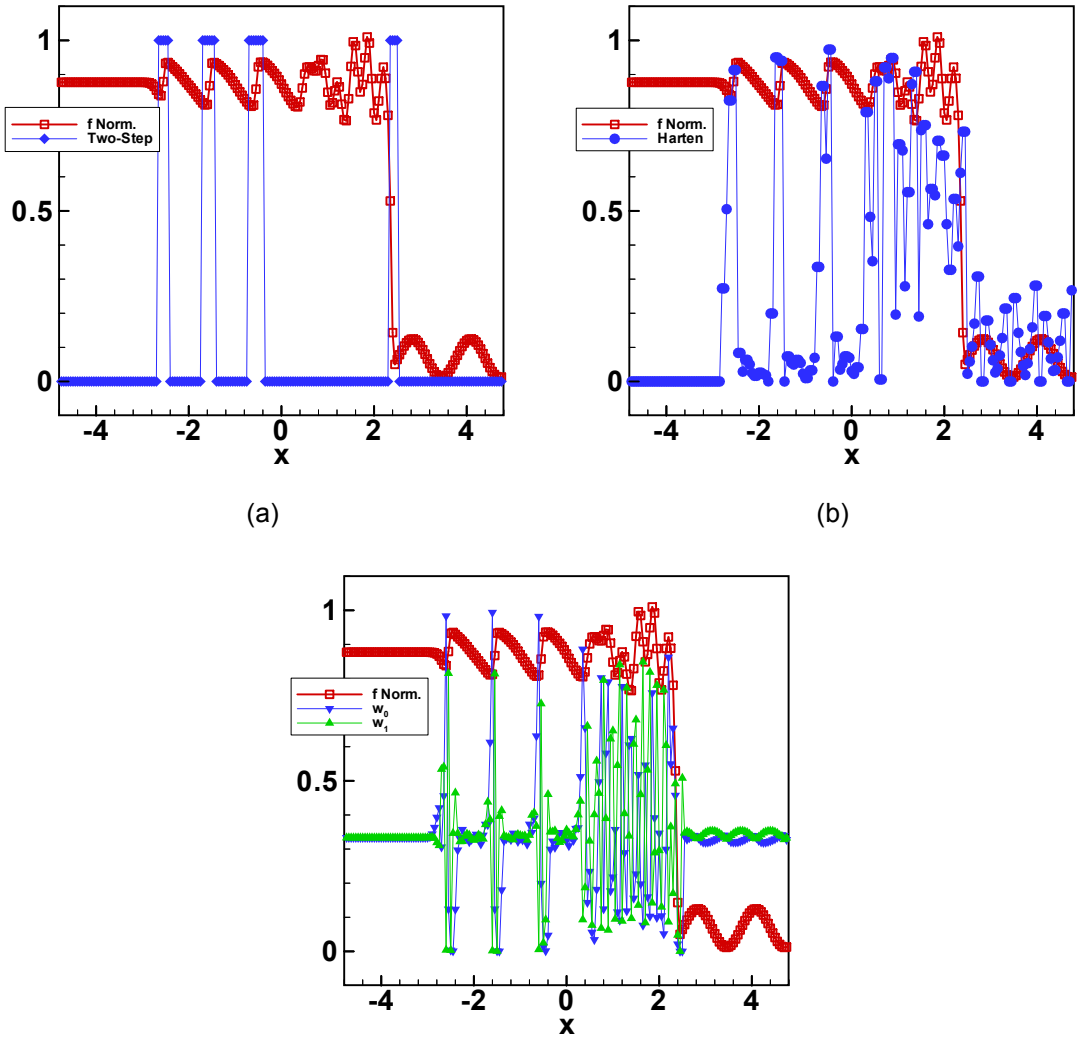

Figure 6.7 Shock detector for 1D shock-entropy wave interaction: (a) Two-step (b) Harten (c) WENO. $w_i = \omega_{i,j+1/2}, i = 0,1$. f is normalized.

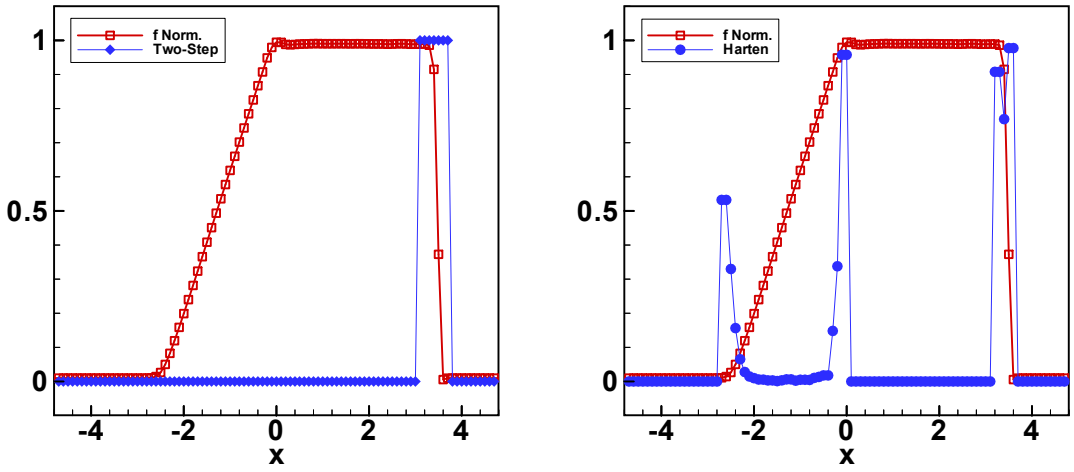

(a)

(b)

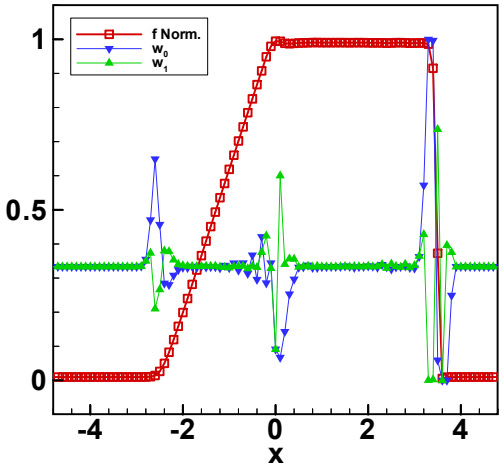

(c)

Figure 6.8 Shock detector for 1D shock tube problem: (a) Two-step (b) Harten (c) WENO. $w_i = \omega_{i,j+1/2}, i = 0,1$. f is normalized.

CHAPTER 7

CONCLUDING REMARKS

In this work, a comparison of the Weighted Compact Scheme and the WENO scheme is performed for one-dimensional applications. It is shown that, individually, each scheme has its own faults, but a linear combination of both schemes improves the final solution. The Weighted Compact Scheme and the WENO scheme have, respectively, no dissipation and too much dissipation in the smooth regions, while they are very efficient in the shock area. The linear combination of both schemes shows that an effective shock detector, together with a high-resolution, low-dissipation scheme and a bias upwind scheme, can be the solution for cases where both shock/discontinuity and small scale lengths are important.

Based on these results, a new shock/discontinuity detector that can effectively capture shocks/discontinuities including strong shocks, weak shocks, and oblique shocks has been developed. The comparison of the new Two-Step detector with the Harten switch function and WENO weights used as detectors show that the latter have difficulty in distinguishing high-frequency waves and critical points from discontinuities, which explains the excessive smearing. The Two-Step detector is robust and does not require adjustment of parameters.

REFERENCES

[1] D. A. Anderson, J. C. Tannehill, and R. H. Pletcher, *Computational Fluid Mechanics and Heat Transfer*, Taylor & Francis, 2nd edition (1997).

[2] G. K. Batchelor, *An Introduction to Fluid Dynamics*, Cambridge University Press (2000).

[3] S.K. Godunov, *A difference scheme for numerical computation of discontinuous solution of hydrodynamic equations*, Math Sbornik 47 (1969), pp. 271–306 (in Russian) translated US Joint Publ. Res. Service, JPRS 7226.

[4] A. Harten, *The artificial compression method for computation of shocks and contact discontinuities: III. self-adjusting hybrid schemes*, Math. Comp. 32(142) (1978), pp. 363–389.

[5] A. Harten, B. Engquist, B. Osher, and S.R. Charkravarthy, *Uniformly high order accurate essentially non-oscillatory schemes III*, J. Comput. Phys. 71 (1987), pp. 231–303.

[6] G.S. Jiang and C.W. Shu, *Efficient implementation of weighted ENO scheme*. J. Comput. Phys. 126 (1996), pp. 202–228.

[7] L. Jiang, H. Shan, and C. Liu, *Weight compact scheme for shock capturing*, Int. J. Comput. Fluid Dyn. 15 (2001), pp. 147–155.

[8] S.K. Lele, *Compact finite difference schemes with spectral-like resolution*, J. Comput. Phys. 103 (1992), pp. 16–42.

[9] D. Liu, S. Osher, and T. Chan, *Weighted essentially non-oscillatory schemes*, J. Comput. Phys. 115 (1994), pp. 200–212.

[10] P. Lu, M. Oliveira, C. Liu, *High-order compact scheme for boundary points*, International Journal of Computer Mathematics, to be published (DOI 10.1080/00207160802506512).

[11] P. Lu, M. Oliveira, C. Liu, *High order compact scheme for Dirichlet boundary points*, Neural, Parallel and Scientific Computations, 16 (2) (2008), pp. 273-282.

[12] M.P. Martin, *Direct numerical simulation of hypersonic turbulent boundary layers. Part 1. Initialization and Comparison with Experiments*, J. Fluid Mech. 570 (2007), pp. 347–364.

[13] M. Oliveira, P. Lu, C. Liu, *A New Shock Detector/Locator*, International Journal of Computer Mathematics, to be published.

[14] M. Oliveira, J. Su, P. Xie, C. Liu, *Truncation error, dissipation and dispersion terms of fifth order WENO and of WCS for 1D conservation law*, International Journal of Computer Mathematics, to be published (DOI 10.1080/00207160802036890).

[15] M. L. Oliveira, P. Xie, J. Su, C. Liu, *Modified Weighted Compact Scheme for Shock-Boundary Layer Interaction and Double Cone*, AIAA Paper AIAA-2008-0755 (2008).

[16] M. Oliveira, P. Lu, X. Liu, C. Liu, *Universal High Order Subroutine with New Shock Detector for Shock Boundary Layer Interaction*, AIAA Paper AIAA-2009-1139 (2009).

[17] P.L. Roe, *Approximate Riemann solvers, parameter vectors and difference schemes*, J. Comput. Phys. 43 (1981), pp. 357–372.

[18] C.W. Shu and S. Osher, *Efficient implementation of essentially non-oscillatory shock-capturing scheme*, J. Comput. Phys. 77 (1988), pp. 439–471.

[19] C.W. Shu and S. Osher, *Efficient implementation of essentially non-oscillatory shock-capturing schemes II*, J. Comput. Phys. 83 (1989), pp. 32–78.

[20] J. Su, M. Oliveira, P. Xie, C. Liu, *Error analysis for weighted higher order*, Applied Mathematical Sciences, 1 (58) (2007), pp.2863-2881.

[21] B. Van Leer, *Towards the ultimate conservative difference scheme. V: A second-order sequel to Godunov's scheme*, J. Comput. Phys. 32 (1979), pp. 101–136.

[22] M. Visbal and D. Gaitonde, *On the use of higher-order finite-difference schemes on curvilinear and deforming meshes*, J. Comput. Phys. 181 (2002), pp. 155–185.

[23] P. Xie, M. L. Oliveira, J. Su, C. Liu, *High Order Weighted Compact Schemes for Shock/Boundary Layer Interaction*, AIAA Paper AIAA-2008-0754 (2008).

BIOGRAPHICAL INFORMATION

Maria Luisa Bambozzi Oliveira has received a Bachelor of Science degree in Physics and a Master of Science degree in Computer Science and Computational Mathematics from the University of São Paulo in Brazil. Her research at the University of Texas at Arlington has earned her a College of Science Dean's Excellence Scholarship and a Department of Mathematics Outstanding Graduate Research Award in the Spring of 2009. Her research interests include the numerical simulation of Navier-Stokes flows.